Thin-Walled Structures 190 (2023) 111015

Contents lists available at ScienceDirect

Thin-Walled Structures

journal homepage: www.elsevier.com/locate/tws

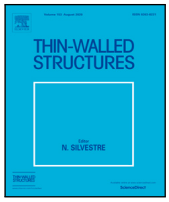

Full length article

# Influence of the designer-assumed cyclic hardening parameters on the overstrength of austenitic stainless steel links

Lucy Lázaro *, Rolando Chacón

*School of Civil Engineering, Department of Civil and Environmental Engineering, Universitat Politècnica de Catalunya, Spain*

ARTICLE INFO

*Keywords:*
Cyclic parameters
Stainless steel
Overstrength
Backstress

ABSTRACT

Dissipative zones in buildings allow for the release of energy when a seismic event occurs. The structural analysis of these zones involves the study of the structure at different levels ranging from mechanical properties of materials, adjacent elements, and the whole system.

The materials, elements and structures require ductility and strength. Within this framework, austenitic stainless steel (ASS), as a material subjected to cyclic fatigue, shows significant strain hardening and ductility. These promising features require an in-depth analysis when used for dissipative zones. For instance, structures such as eccentrically braced frames (EBFs), whose dissipative zones are placed in links, need that these links achieve the plastic stage first whereas the adjacent elements remain in the elastic stage.

The overstrength within the numerical design of structures deserves particular attention, as do the factors involved in the modelling that can affect its assumption.

Particularly, a study of the way of cyclic hardening parameters are used can influence the overstrength ASS was carried out. Three ways were considered: average, single values and the superposition of eight backstresses for kinematic hardening. The last one revealed the most conservative results and a higher influence on the link overstrength.

It was found that the designed-assumed cyclic parameters directly influenced the link overstrength. With the designed-assumed that considered several changes to the kinematic hardening, the link overstrength was higher with less energy dissipated. Nonetheless, the link's ductility and dissipated energy increased when the hardening was regular. The experimental material validation and numerical results of the EBF with ASS links were similar.

## 1. Introduction

Seismic events have called the attention of the structural engineering research community for decades. The goal to prevent serious damage to a building has led to manifold seismic-resistant structural types and materials. A way to prevent damage in seismically exposed structures is through the dissipation of energy in predetermined zones of a building. In frames, these zones denominated dissipative zones are placed according to their dissipation mechanism. These zones are designed to achieve the plastic stage earlier than their adjacent elements (principle of hierarchy of resistances). Eccentrically braced frames (EBFs), which are conformed by columns, braces, beams, and links, are meant to dissipate energy through shear or shear-bending mechanisms produced specifically at the structural links, the elements that are designed as dissipative.

Austenitic stainless steel shows considerable strain hardening and ductility when subjected to low and extremely low cycle tests, which can also be observed in [1–3]. In addition, experimental studies in different structural elements under cyclic loading have been developed [4,5] showing a greater ductility, high strain hardening and local buckling prior to failure of the element of SS. Frames assembled by SS members are also under study and results demonstrate their viability [6–9].

ASS links are assessed as a potential alternative when placed in strategic zones within frames, i.e. dissipative zones, which, when a seismic event occurs, release energy through a mechanism (flexural, shear or a combination of both). The overstrength of the members is assessed for the consideration of a thorough design in these zones using ASS.

At the moment, the systematic use of adequate cyclic parameters for ASS is not clear. Selecting a specific set of cyclic strain hardening parameters results on rather different responses. In this study, a widespread evaluation of the influence of the use of cyclic parameters mainly on overstrength, was developed. The study is aimed at giving guidance to designers for a more rational and adequate selection of those parameters when analysing ASS as part of vaster systems such as eccentrically braced frames.

* Corresponding author.
*E-mail address:* lucy.laura.lazaro@upc.edu (L. Lázaro).

https://doi.org/10.1016/j.tws.2023.111015
Received 1 December 2022; Received in revised form 27 May 2023; Accepted 8 July 2023
Available online xxxx

The principal objective of this research is to determine how the designer-assumed cyclic parameters influence the key features of hybrid EBF links. Specifically, this study aims to examine the effects of kinematic hardening on the cyclic behaviour of the link as a fuse element.

The cyclic parameters for this study were selected from the previous experimental tests of ASS. Following this, specimens with arbitrary loadings were modelled primarily using kinematic hardening variations, since this type of hardening was observed in scattered results during experimental testing.

## 2. Literature review

According to EN1998-1 [10], the classification of seismic frames is the following: Moment Resisting Frames (MRF), Concentrically-Braced Frames (CBF) and Eccentrically-Braced Frames (EBF). The last one has gained importance since its fuse element can be even replaced after a seismic event if damaged. EBFs have been studied within the framework of both capacity- and performance-based design.

EBFs are structural systems consisting of columns, beams, braces and a special element that works as a fuse, namely a link. These elements can be located in different ways (i.e. horizontal, vertical, in the middle or the extreme of the beams). When an EBF undergoes certain horizontal loading, it mainly dissipates energy through a shear force developed in the link element.

In the framework of "capacity design" EN1998-1 [10] introduce two principles for the design of structures, the first one concerns dissipative zones and limit states that must be designed according to the maximum internal actions. The second refers to non-dissipative zones whose behaviour must be able to support the maximum internal actions elastically.

A desired behaviour of EBFs is when the link achieves the plastic stage, while adjacent elements remain in an elastic range. In this context, the overstrength of links is a key characteristic. According to 2005 AISC seismic provisions [11], the maximum shear capacity of a link (Vu) can be calculated as:

$$V_u = \Omega R_y V_n \tag{1}$$

where $R_y$ is the overstrength factor due to material randomness defined by the ratio of expected and nominal yield strength, $V_e = R_y V_n$ is the expected shear capacity of the link, $V_n$ is the nominal shear capacity of the link, and $\Omega$ is the overstrength due to strain hardening. The values for this factor are being studied; EN 08 and AISC 341 seismic provisions propose a constant value for the link overstrength made of carbon steel.

An important geometrical feature is the link length coefficient $\rho$, which depends on the type of failure mechanism. This coefficient is determined by $\rho = eV_p/M_p$ where $e$ is the length of the link, $M_p$ is the plastic moment and $V_p$ is the shear capacity of the link. When $\rho < 1.6$, the links are labelled short and their failure mechanism is shear. If $\rho > 2.6$, the links are called long and their failure is flexure. For $1.6 < \rho < 2.6$, the links are termed intermediate and their failure is both shear and flexure.

Recent studies showed the influence of different mechanical and geometrical features, which demonstrated that this value requires further inspection. The influence of these characteristics on the link overstrength factor has been analysed. It is shown that the overstrength increases when the web aspect ratio $e/h_w$ decreases [12], the same behaviour was observed when the ratio of link length and cross-section depth $e/d$ decreases [13]. Besides, as the web height-thickness ratio $h_w/t_w$ reduces, the ultimate overstrength factor increases [12].

Experimental results from the literature reveal interesting conclusions for carbon steel (CS), Azad et al. [14] noted that for $\rho > 1$ the overstrength factor seems to be reasonable with the value adopted for AISC 341. Ji et al. [15] found higher values of overstrength in very short links with $\rho < 1$, therefore, the constant value of the $\Omega$ was found inadequate. For long links $\rho > 1$, Yasin O. [16] found overstrength factors significantly higher than the assumed values in AISC 341. Okazaki et al. [17] developed tests with short, intermediate, and long links and established that the overstrength factor of short links was higher than for the intermediate and long links.

On the other hand, the influence of axial forces and restraints on the overstrength factor has also been evaluated. Dalla Corte et al. [13] mentioned that tensile axial forces due to restrain to axial deformations and nonlinear geometric effects combined with the ratio of flange over web area and the aspect ratio modify the overstrength factor. X. Liu et al. [12] and L. Manganiello et al. [18] studied the nonlinear geometric effect of axial restraints on the overstrength of short links in different types of steels and found that when the axial utilisation rate increases the overstrength factor does increase as well.

Developing a focused scrutiny on several studies from the literature, Manganiello et al. [18] and Mohebkhah et al. [19] concluded that the overstrength factor is influenced by the following factors: flange-web area ratio or shear resistance of flanges, link length coefficient ($\rho$), loading protocol and the presence of axial forces due boundary axial restraints. All these geometrical factors were assessed for CS.

Regarding the material behaviour, strain hardening affects directly shear link overstrength. Therefore, the designer-assumed parameters of the cyclic behaviour of the material that is needed for proper numerical modelling are worth assessing as well.

W. Yin et al. [20] analysed the contribution of isotropic and kinematic hardening for low yield point steel and used the Chaboche model [21] to characterise the kinematic–isotropic combined hardening, which employed the superposition of four backstresses in kinematic hardening. Xiao et al. [12] studied Q345GJ steel in shear links, which showed good ductility and rare cyclic hardening with hardly isotropic and significant kinematic hardening. Additionally, this material was characterised by four non-lineal kinematic hardening. The use of superposition of four kinematic hardening in the aforementioned studies has as precedent the research of J.L. Chaboche [22] who investigated the cyclic behaviour of stainless steel with four superpositions of kinematic hardening with relatively satisfactory results.

As well as with low yield steel, high-strength steel or Q345GJ steel are utilised in shear links, austenitic stainless steel (ASS) is considered in links, the resulting and the factors that influence the overstrength deserves a thorough analysis.

In monotonic tests, austenitic stainless steel leaves the linear stage prior to carbon steel. Nevertheless, cyclic experimental tests [23,24] show that this material possesses a higher strain hardening and ductility. These features have attracted the attention in seismic design, particularly in dissipative zones of frames. Both benefits and concerns draw the attention of the research community.

Di Sarno et al. [25] were one of the first researchers to study seismic resistant frames with SS in braces and links. Their findings exhibited good plastic deformations, excellent energy absorbing capacity, and a strain hardening nearly twice that of carbon steel. However, the SS was modelled on the base of the uni-axial Ramberg–Osgood formulation, i.e. with the consideration of the monotonic behaviour of SS.

Additionally, Li et al. [26] performed a numerical study of the cyclic behaviour of austenitic stainless steel in shear links and characterised the material through the combined strain hardening rule, They used two superimposed kinematic hardening according to the Chaboche model and isotropic hardening as per Voce hardening law.

Another preliminary study was carried out using austenitic SS in dissipative zones of EBFs. Chacon et al. [27] developed a numerical study on links of SS and used cyclic parameters from the combined Chaboche model to characterise the material. They employed the average values of cyclic parameters proposed by K. Nip et al. [1].

Yiwen Wu et al. [28] studied the behaviour of diagonally stiffened stainless steel using the constitutive model proposed by Rasmussen [29] to characterise the monotonic behaviour, the combined model with kinematic and isotropic components to characterise the cyclic behaviour, and the skeleton curve to develop a parametric study.

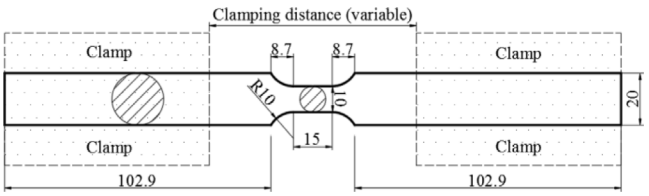


**Fig. 1.** Geometry of specimens (measures are in mm).

J.D. Gao et al. [30] researched the cyclic structural behaviour of austenitic stainless steel and used the cyclic parameters proposed by Chang et al. [31] with the superposition of four kinematic components to obtain the numerical model.

This brief literature review shows the need on understanding the influence of the cyclic hardening parameters (designer-assumed) on the global overstrength of EBFs subjected to cyclic loading.

On the other hand, there are other methods to dissipate energy in EBFs and centrically fused braced frames (CFBF) using the capacity design [32–34], whose mechanical benefits are similar. Currently, the main difference is in the cost of implementation and maintenance during their service life. In this aspect, further studies are necessary.

## 3. Stainless steel EN 1.4307 subjected to seismic loading

Austenitic SS has greater ductility than duplex and ferritic SS [35]. Besides, experimental tests show that this material possesses greater toughness than mild steel [36]. The results of the studies mentioned above stemmed from monotonic tests and the results of austenitic SS subjected to low cycle fatigue showed a significant cyclic strain hardening. In the frame of a recently finished research national project (PINOX-AC). An extensive experimental programme was carried out to determine the cyclic behaviour of EN 1.4307 austenitic SS. A total of 37 coupons were successfully tested. Fig. 1 depicts the geometry of the specimens. The loading protocol was strain controlled. Protocols of constant amplitude (Fig. 2a), multiple step (Fig. 2b) and arbitrary variation of strain amplitudes (Fig. 2c) were performed. A special test with constant strain amplitudes as a history of straining or pre-strain was developed, which was subsequently subjected to arbitrary strain amplitudes (Fig. 2d).

The results of this study confirm the high cyclic strain hardening and ductility already observed in previous and recent studies [2,24,37–39]. This detailed experimental work, which calibrated the cyclic material property utilised in this study, is also described in previously research by the authors of this paper [23].

## 4. Validation of results of the material

The development of the aforementioned tests was validated using Abaqus-Simulia. The results of this validation are shown in Fig. 3. To model the Bauschinger effect of austenitic stainless steel, the combined Chaboche model, implemented in Abaqus was used. This model is based on the a combination of isotropic and kinematic components. The isotropic component represents the increase of the yield surface and the kinematic component represents the movement of the yield surface. This model, however does not represent fracture.

A coupon identical to the ones tested experimentally was modelled using solid finite elements. The parameters obtained from the experimental programme previously developed [23] were used for numerical models. Fig. 3 illustrates the comparison between experimental and numerical data for a 3% of applied strain amplitude with close agreement.

The C3D8R finite element was employed to perform the numerical model and the mesh with the better result was of 3 mm in size. The ends of the specimens were fixed to simulate the clamps of the testing machine.

Another numerical study was developed with the results. As shown in Fig. 2c, arbitrary strain, which consisted of several no-constant amplitude cycles, was considered as a target protocol to study the material behaviour. When the protocol establishes a given strain value (or known), designers tend to select parameters for that specific value. However, in an arbitrary strain protocol, at first sight, it is uncertain which values of cyclic parameters should be used. Designers might consider the values corresponding to the maximum strain, the average strain, or the minimum strain applied. To ignite such debate at material levels, different values were selected and the results are shown in Fig. 4a to d.

In Fig. 4a, the average values of the cyclic parameters from the experimental data were used, the results showed a good agreement and the maximum achieved numerical stress was 4.5% minor than the

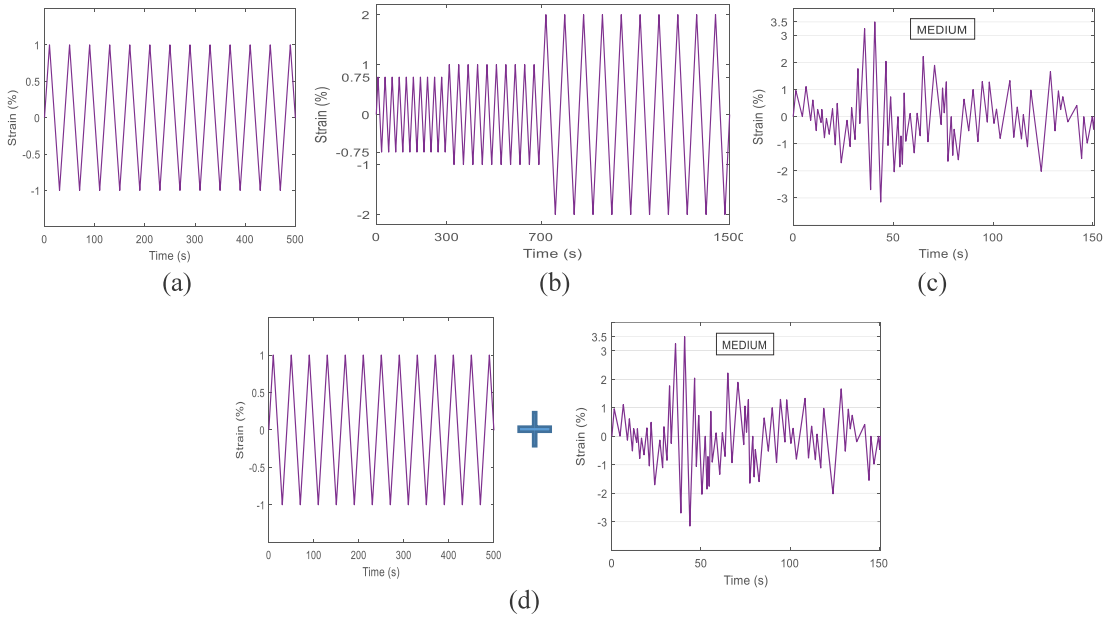


**Fig. 2.** Strain protocol applied to the specimens.

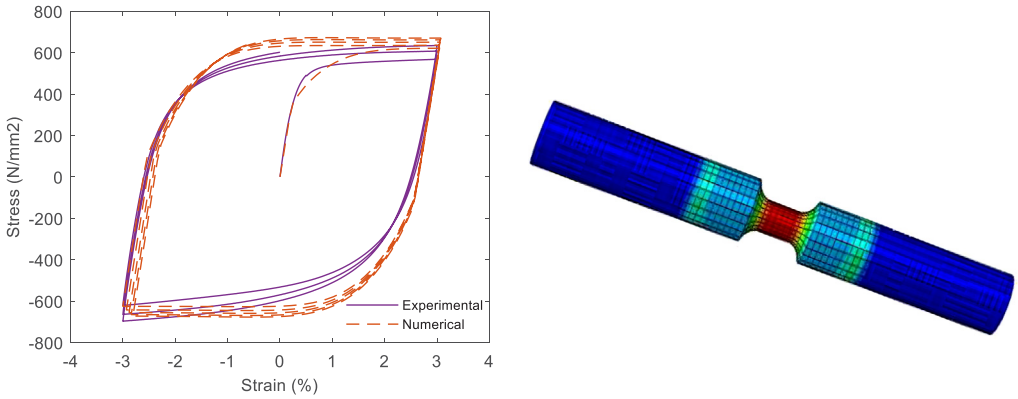


**Fig. 3.** Comparison between experimental and numerical model for 3% of constant applied strain.

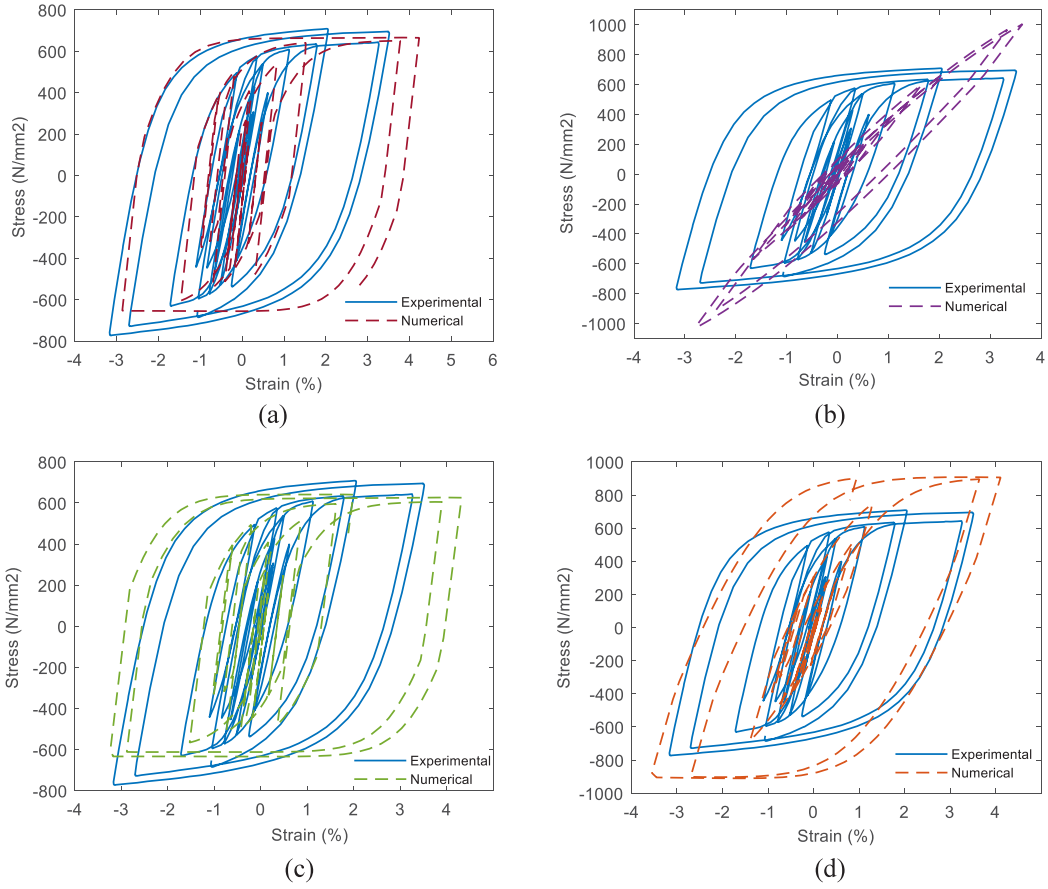


**Fig. 4.** Comparison between experimental and numerical model for arbitrary amplitude strain applied.

experimental stress. The hysteresis curve, in this case, was uniform, regular and similar to experimental data.

In Fig. 4b, all cyclic parameters from experimental results were used (eight sets of cyclic parameters according to the strain applied). Abaqus employed the combined Chaboche model with one increase of the yield surface (isotropic component) and the superposition of a maximum of ten backstresses to kinematic component.

The results from the comparison between experimental and numerical data showed that although the numerical strain was almost similar to the experimental strain, the numerical hysteresis curve do not coincide. The movement of the yield surface was clearly observed in the numerical model.

In Fig. 4c, cyclic parameters correspond to the maximum strain applied, i.e. one isotropic and kinematic component for 3% of strain amplitude. The comparison between the numerical and experimental hysteresis curves showed a good agreement and the maximum achieved numerical stress was 9.5% minor than the experimental stress. The numerical results developed higher difference in the strain achieved with a maximum strain of 4.32%.

Finally, in Fig. 4d, we used four backstresses to the kinematic component, which belonged to cyclic parameters from 1%, 2%, 2.5%, and 3%. It is worth mentioning that the values were smaller than the maximum strain applied. The strain achieved was almost similar; however, the numerical stresses were higher than the experimental stresses.

Furthermore, it was obtained the maximum values achieved in each irregular cycle and compared with the numerical results presented in Table 1, where the negative sign (−) indicates that the specimen was

**Table 1**
Maximum values achieved in each irregular cycle.

| Experimental | | Numerical- average | | Num/Exp (%) | |
|---|---|---|---|---|---|
| Strain (%) | Stress (N/mm2) | Strain (%) | Stress (N/mm2) | Strain | Stress |
| 1.12 | 597.50 | 0.83 | 539.10 | 73.74 | 90.23 |
| 1.77 | 634.00 | 1.52 | 640.40 | 85.92 | 101.01 |
| 3.26 | 632.20 | 3.78 | 649.90 | 115.66 | 102.80 |
| 3.49 | 695.50 | 4.23 | 664.80 | 121.19 | 95.59 |
| −0.51 | −526.50 | −0.35 | −496.70 | 68.28 | 94.34 |
| −0.77 | −569.70 | −0.71 | −543.40 | 91.90 | 95.38 |
| −1.69 | −629.90 | −1.47 | −604.80 | 86.58 | 96.02 |
| −2.70 | −718.50 | −2.86 | −652.80 | 106.04 | 90.86 |
| Experimental | | Numerical- single | | Num/Exp (%) | |
| Strain (%) | Stress (N/mm2) | Strain (%) | Stress (N/mm2) | Strain | Stress |
| 1.12 | 597.50 | 0.81 | 505.50 | 72.12 | 84.60 |
| 1.77 | 634.00 | 1.61 | 595.70 | 91.12 | 93.96 |
| 3.26 | 632.20 | 3.90 | 604.90 | 119.39 | 95.68 |
| 3.49 | 695.50 | 4.32 | 625.70 | 123.77 | 89.96 |
| −0.51 | −526.50 | −0.43 | −497.50 | 84.15 | 94.49 |
| −0.77 | −569.70 | −0.74 | −517.00 | 96.48 | 90.75 |
| −1.69 | −629.90 | −1.53 | −566.30 | 90.31 | 89.90 |
| −2.70 | −718.50 | −2.88 | −611.50 | 106.67 | 85.11 |
| Experimental | | Numerical- 4Backs | | Num/Exp (%) | |
| Strain (%) | Stress (N/mm2) | Strain (%) | Stress (N/mm2) | Strain | Stress |
| 1.12 | 597.50 | 0.81 | 494.70 | 72.68 | 82.79 |
| 1.77 | 634.00 | 1.29 | 746.60 | 72.91 | 117.76 |
| 3.26 | 632.20 | 3.64 | 895.90 | 111.64 | 141.71 |
| 3.49 | 695.50 | 4.11 | 906.30 | 117.86 | 130.31 |
| −0.51 | −526.50 | −0.58 | −431.60 | 114.75 | 81.98 |
| −0.77 | −569.70 | −0.75 | −500.43 | 97.24 | 87.84 |
| −1.69 | −629.90 | −1.39 | −682.10 | 82.33 | 108.29 |
| −2.70 | −718.50 | −2.69 | −901.00 | 99.44 | 125.40 |
| Experimental | | Numerical- 8Backs | | Num/Exp (%) | |
| Strain (%) | Stress (N/mm2) | Strain (%) | Stress (N/mm2) | Strain | Stress |
| 1.12 | 597.50 | 1.15 | 412.10 | 102.41 | 68.97 |
| 1.77 | 634.00 | 1.65 | 598.60 | 93.21 | 94.42 |
| 3.26 | 632.20 | 3.33 | 967.10 | 102.14 | 152.97 |
| 3.49 | 695.50 | 3.64 | 1004.00 | 104.21 | 144.36 |
| −0.51 | −526.50 | −0.39 | −185.20 | 77.04 | 35.18 |
| −0.77 | −569.70 | −1.01 | −374.20 | 131.08 | 65.68 |
| −1.69 | −629.90 | −1.66 | −564.20 | 98.17 | 89.57 |
| −2.70 | −718.50 | −2.39 | −908.00 | 88.37 | 126.37 |

under compression. The best results were achieved by applying a 3% strain and using the average values of the cyclic parameters, i.e., when the kinematic hardening was regular without changes.

It is worth pointing out that the cyclic parameters shown in [23] stemmed from the companion strain protocol (Fig. 2a) and were calculated and calibrated for each strain amplitude applied, i.e. one isotropic and kinematic component for strain amplitude. From the validation of the results mentioned above, a designer should bear in mind that adequate cyclic parameters are related to expected achievable strain levels, which is a difficulty since the designer-assumed conditions depend on the response obtained.

## 5. Numerical study on eccentrically braced frame

### 5.1. Previous considerations

This investigation aims to evaluate how cyclic parameters affect the cyclic behaviour of a hybrid EBF at both the element and structure levels, based on experimental test results of the material (ASS).

The selected element was the link, and the structure was a simple hybrid EBF with dimensions taken from [40]. While [40] studied an EBF with five storeys and one bay made entirely of carbon steel, this study only focuses on one storey, and the link is made of ASS with cyclic properties obtained from previous material tests.

The links were preselected to dissipate energy through the shear failure mechanism, i.e., using short links. The beams were selected with similar section areas to the links to simulate a continuous connection, and the braces were equal to the beams. Columns ensured the stiffness of the structure and capacity design.

### 5.2. Description of eccentrically braced frames studied

An extensive numerical study was conducted to determine how the use of cyclic parameters affects the response of short links with varying web slenderness. Under this goal, 216 models were analysed. The geometric characteristic is as follows.

The studied EBFs have one bay and one storey with a horizontal link. The bay is 9 m, and the storey is 5.45 m high for all models. Fig. 5 illustrates the configuration and measures obtained from a referenced structure [40] and with gravitational loads indicated in Fig. 5. The referenced EBF is adapted to be hybrid, i.e., austenitic SS EN 1.4307 for links and carbon steel S355 (CS) for columns, beams, and braces. That is to say, dissipative zones are designed with SS whereas non-dissipative zones are designed with CS.

The conducted parametric study includes different types of cross-sections of links developed from a variation of geometries on standard profiles ranging from HEA240 to HEA400. The base geometry was used with variations of the thickness, which resulted in non-Standard sections. The length of the links ranged from 1000 to 1400 implying that the link length coefficient is $\rho < 1.6$ and the link is expected to fail under a pure shear mechanism. This variation was motivated by the analyses of a representative range of short links. Table 2 depicts the geometric properties of the structural elements.

The geometric parameter used in this study was the ratio of link web-thickness over beam web-thickness ($t_{wL}/t_{wB}$); thereby web links were thinner or equal than web beams. The link flange thickness remained with values from Table 2.

Three values for $t_{wL}/t_{wB}$ were selected. The first one $t_{wL}/t_{wB} = 1$ stands for $t_{wL} = t_{wB}$; the second one, for $t_{wL}/t_{wB} = 0.9$ that is $t_{wL} < t_{wB}$, and finally $t_{wL}/t_{wB} = 0.8$ i.e. $t_{wL} \ll t_{wB}$.

The cyclic parameters represent a key part of the study addressed in the section corresponding to inelastic dynamic analysis. The models were labelled according to the cross-section, the thickness of the link and the type of displacement applied. HEA240-M7.5 represents an EBF with an HEA240 link, beam and braces, M stands for monotonic applied load and 7.5 for 7.5 mm of link web thickness. It is worth mentioning that the variation of ratio $t_{wL}/t_{wB}$ was through the variation of link thickness while, the beam thickness remained constant.

## 6. Structural analysis

Inelastic static and inelastic dynamic analyses were performed using Abaqus Simulia [41]. Beams, columns, and braces were modelled as beam B31 type element and a mesh size of approximately 80 mm. The links were modelled with shells (S4R5 type) and a mesh size of roughly 40 mm. An additional analysis was developed to compare another model using shell elements in beams, columns and braces and the results were satisfactorily similar. Therefore, the combination of beam B31 and shell S4R5 was selected to reduce the computational time. Geometric and material nonlinearities were considered in models.

The evaluation of adequate size mesh was carried out through the buckling analysis; the parameters valued were the computational time and the better approximation. Table 3 depicts the analysis, which starts at 100 mm and finishes at 5mm whose results allowed the selection of the optimal size of 40–30 mm Fig. 6 with a computational time of 18 and 24 seconds respectively.

Therefore, to achieve the size mesh selected (40–30 mm) the following number of elements was used in shell links:

- 30 elements in the depths of the web and 14 elements in the flanges in the HEA240, HEA260, and HEA280 sections.

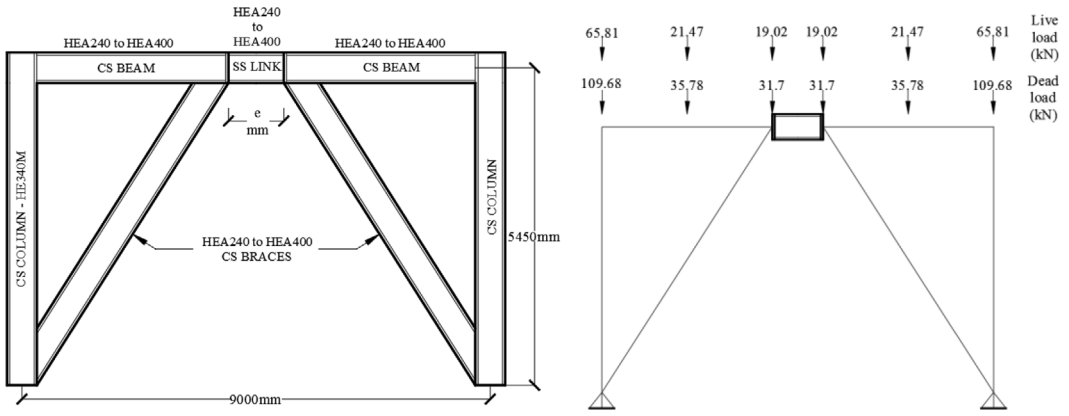


**Fig. 5.** Geometry and gravitational load applied frames.

**Table 2**
Geometric properties of the structural elements.

| Section | dw (mm) | b (mm) | $t_{wL}$ (mm)* for $t_{wL}/t_{wB} \approx 0.8$ | $t_{wL}$ (mm)* for $t_{wL}/t_{wB} \approx 0.9$ | $t_{wL}$ (mm)* for $t_{wL}/t_{wB} = 1$ | $t_{wB}$ (mm) | $t_f$ (mm) | e (mm) | $\rho$ |
|---|---|---|---|---|---|---|---|---|---|
| HEA240 | 240 | 240 | 6 | 7 | 7.5 | 7.5 | 12 | 1000 | 1.5 |
| HEA260 | 260 | 260 | 6 | 7 | 7.5 | 7.5 | 12.5 | 1200 | 1.6 |
| HEA280 | 280 | 280 | 6.5 | 7.5 | 8 | 8 | 13 | 1200 | 1.52 |
| HEA300 | 300 | 300 | 7 | 8 | 8.5 | 8.5 | 14 | 1300 | 1.52 |
| HEA320 | 320 | 300 | 7.5 | 8.5 | 9 | 9 | 15.5 | 1400 | 1.56 |
| HEA340 | 340 | 300 | 8 | 9 | 9.5 | 9.5 | 16.5 | 1400 | 1.55 |
| HEA360 | 360 | 300 | 8 | 9.5 | 10 | 10 | 17.5 | 1400 | 1.54 |
| HEA400 | 400 | 300 | 9 | 10 | 11 | 11 | 19 | 1400 | 1.56 |
| HE340M | 377 | 309 | 21 | 21 | 21 | 21 | 40 | – | – |

*Standard thickness.

**Table 3**
Mesh size and computational time.

| Mesh size | Eigen value (N) | Computational time (s) |
|---|---|---|
| 100 mm | 1.20E+06 | 16 |
| 70 mm | 1.04E+06 | 18 |
| 50 mm | 9.68E+05 | 18 |
| **40 mm** | **9.38E+05** | **18** |
| **30 mm** | **9.19E+05** | **24** |
| 20 mm | 9.04E+05 | 26 |
| 10 mm | 8.96E+05 | 59 |
| 5 mm | 8.94E+05 | 168 |

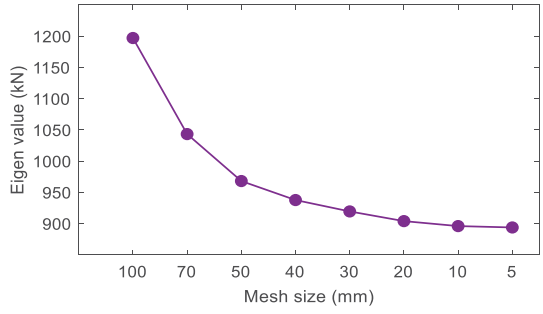


**Fig. 6.** Mesh analysis.

- 38 elements in the depths of the web and 18 elements in the flanges in the HEA300, HEA320, and HEA340 sections.
- 48 elements in the depths of the web and 24 elements in the flanges in the HEA360 and HEA400 sections.

The interaction between the shell links and wire beam was performed through a kinematic coupling type in each link ends (Fig. 7). Therefore, the connection between the beams and the link was considered continuous.

**Table 4**
Imperfection values.

| Cross-section | Imperfection value (mm) | Magnitude |
|---|---|---|
| HEA400 | 2 | min (e/200, b/200) |
| HEA360 | 1.8 | 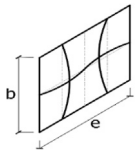 |
| HEA340 | 1.7 | |
| HEA320 | 1.6 | |
| HEA300 | 1.5 | |
| HEA280 | 1.4 | |
| HEA260 | 1.3 | |
| HEA240 | 1.2 | |



Subsequently, a buckling analysis was carried out. Global buckling was observed when applying a load in the control point and the first mode was developed in braces and beams. Local buckling was studied in models in which unitary displacements were applied in opposite directions at the ends of the link.

The initial imperfections were considered according to Annex C of Eurocode 3 [42]. As the focus of this analysis is the cyclic behaviour of the link within the EBF, the local imperfection of the link has been taken into account. The values used for the parametric study corresponded to first buckling modes (Fig. 8), and they were scaled by the values of Table 4. The ends of the links were considered as rigid through coupling constrain in the middle of the ends, which allowed the application of the unitary load to model the local buckling. Fig. 8 shows the first buckle mode for HEA240 and HEA400 models. Out-of-plane displacements in four waves (shear related) are observed for these specific examples.

### 6.1. Inelastic static analysis

The target of this analysis was to find out the response of the link, the beams and the base shear due to a horizontal monotonic displacement applied in a corner of the roof (Fig. 9). The magnitudes

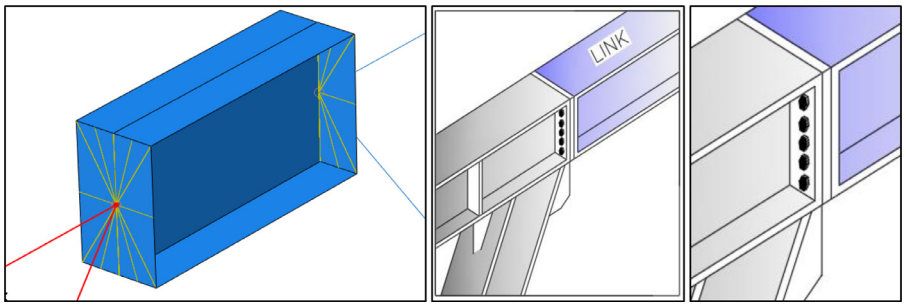


**Fig. 7.** Interaction and connection between link and beams.

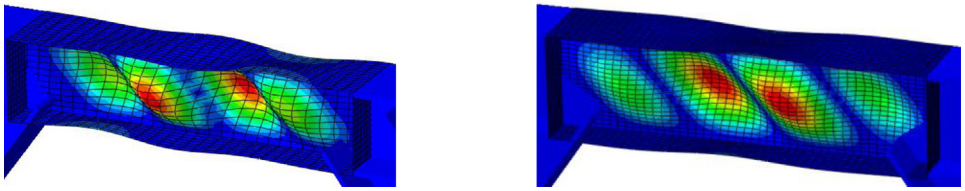


**Fig. 8.** First buckle mode for HEA240-M6 and HEA400-M9 models.

**Table 5**
Mechanics properties of materials.

| (a) Elastic properties | | |
|---|---|---|
| Material | Modulus of elasticity E (N/mm $^2$) | Poisson U |
| CS S355 | 21 0000 | 0.3 |
| AUST SS | 18 4152.7 | 0.3 |

(b) Parameters of combined isotropic/kinematic hardening model of cyclic plasticity (average values from [23])

| Material | $\sigma_o$ (N/mm $^2$) | Ck (N/mm$^2$) | $\gamma$k | $Q_\infty$ | b |
|---|---|---|---|---|---|
| Austenitic SS | 360 | 53 611 | 185 | 111 | 1.56 |

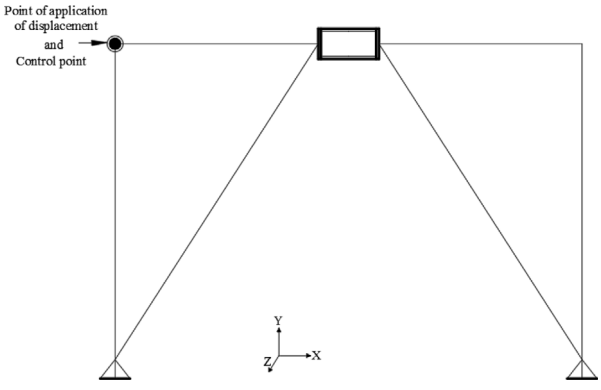


**Fig. 9.** Location of applied displacement and control point.

of the applied displacement were 200 mm and 500 mm, which were selected to reach the failure of the EBF.

The mechanical properties of carbon steel and austenitic stainless steel are specified in Table 5. The plastic properties for stainless steel, which were extracted from experimental results and are detailed in [23].

### 6.2. Inelastic dynamic analysis

The analysis aims to understand the cyclic behaviour of a SS link within a simple EBF and to determine the influence of cyclic parameters on the overstrength of the member.

Three cyclic displacements of constant amplitudes, whose values were obtained from the inelastic static analysis. That is to say, displacements were read from the monotonic response when plastic deformation reached 1%, 3% and 5% at the link. To characterise the cyclic behaviour of SS, the combined Chaboche model, which possesses an isotropic and kinematic hardening component, was used.

Three variations of the form of utilisation of cyclic parameters were applied. The first one corresponds to the single values obtained experimentally for the specific cyclic tests of 1%, 3% and 5% found in [23] (Table 6a). The second one to the average of all values obtained for different strain levels (Table 5b), and the last one to the superposition of eight of kinematic hardening backstresses (Table 6b).

As a matter of fact, when analysing the structural cyclic response of a SS member, the designer needs to select a set of cyclic parameters. This represents a major assumption. This study investigates the consequences of this selection on the response of the links.

As mentioned in Section 4, although the material validation revealed a high scatter when several backstresses were used, in this section that analysis will be developed to confirm the same results in the case of ASS in structural elements subjected to cyclic displacements.

The models were labelled in agreement with the cross-section type, the thickness of the link, the type of the applied displacement, the strain amplitude, and the type of variation of cyclic hardening parameters utilised. To identify the type of cyclic parameters, capital letters were used. A for average values, B for eight superposition of kinematic hardening, and U for a single parameter. Some examples of this labelling would be HEA240-D0.8–3 A, which represents EBF with an HEA240 link; D which stands for dynamic applied displacement; 0.8 for $t_{wL}/t_{wB}$ = 0.8 ratio; 3 for 3% of strain amplitude; and A for the average of cyclic hardening parameters.

## 7. Results and discussion

### 7.1. Inelastic static analysis

The lateral resistance capacity of 24 EBFs was investigated by inelastic static analysis, whose results demonstrated that links had a desired

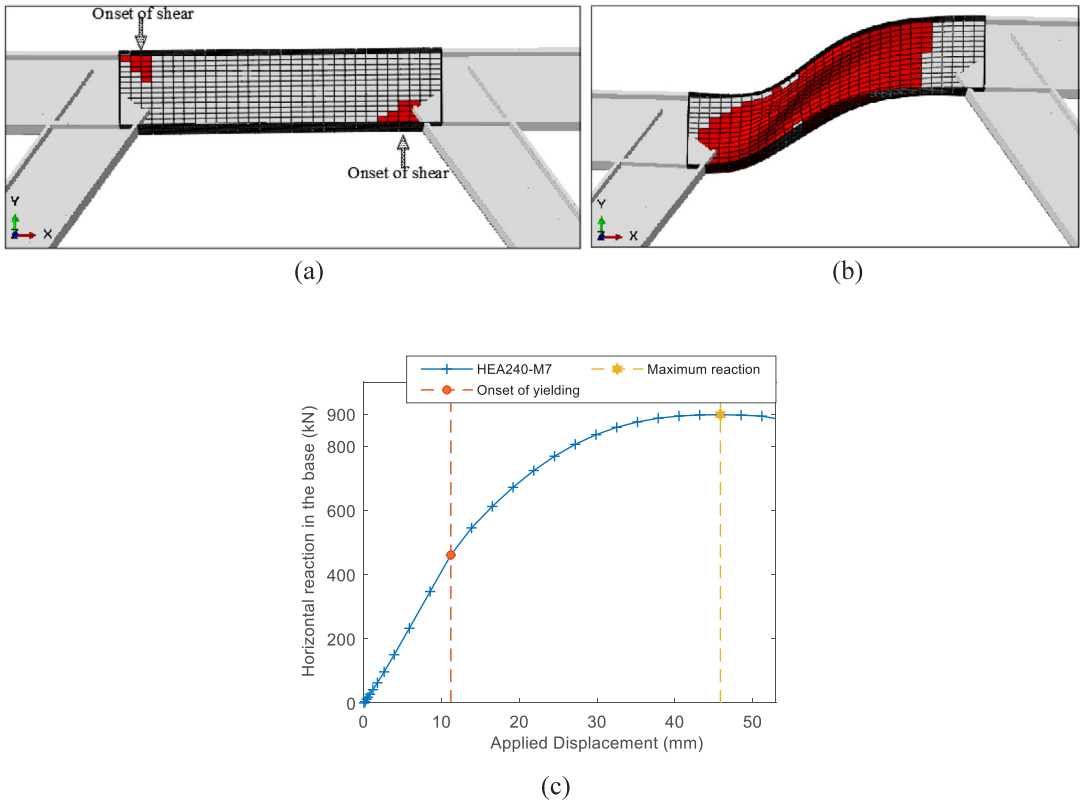


**Fig. 10.** Horizontal reaction in the base and deformation of the link.

**Table 6**
Mechanics properties of materials.

| (a) Specific or single values | | | | | |
|---|---|---|---|---|---|
| Strain amplitude | $\sigma_o$ (N/mm$^2$) | Ck (N/mm$^2$) | $\gamma$k | $Q_\infty$ | b |
| 1% | 368 | 56 622 | 307 | 101 | 0.28 |
| 3% | 352 | 46 645 | 191 | 127 | 1.94 |
| 5% | 419 | 47 692 | 131 | 149 | 131 |

| (b) Eight backstresses for kinematic hardening | | | | | |
|---|---|---|---|---|---|
| Strain amplitude | Ck (N/mm$^2$) | $\gamma$k | $\sigma_o$ (N/mm$^2$) | $Q_\infty$ | b |
| 0.75% | 77 270 | 70 | 360 | 111 | 1.56 |
| 1% | 56 622 | 307 | | | |
| 2% | 59 235 | 226 | | | |
| 2.5% | 51 750 | 215 | | | |
| 3% | 46 645 | 191 | | | |
| 3.5% | 50 175 | 181 | | | |
| 4% | 39 500 | 157 | | | |
| 5% | 47 692 | 131 | | | |

behaviour and failed through shear in all models, which confirms the classification of links by the link length coefficient $\rho < 1.6$. The geometrical configurations of EBFs confirms the boundary conditions adopted by different authors [27,43] for isolated links. The main results are discussed as follows.

*Yielding of the link*

In most models, the link web yielded first and subsequently the beams and braces. The yielding started in opposite corners of the link web, as Fig. 10a illustrates, which indicates the initiation of shear failure. When the horizontal reaction in the base achieved its maximum, the link web yielded entirely. Beyond the peak reaction, the link failed by shear mechanism (Fig. 10b)

Fig. 10c shows the curve strain — reaction of the EBF with the HEA240 link. The onset of the yielding was approximately in 10 mm of displacement applied in the control point, the maximum horizontal reaction was approximately in 47 mm and the reaction suddenly decreased in 55 mm of applied displacement.

The applied strain in the cyclic analysis was in form of the shear angle of the link determined by dividing the vertical displacement of both link ends by the length of the link. Fig. 11 illustrates the shear angle in the links due to the applied displacement.

It was assessed as strain in the dynamic analysis of 1% for a shear angle of 0.01 rad, 3% for a shear angle of 0.03 rad, and 5% for a shear angle of 0.05 rad.

The geometric configuration of the EBFs ensured the desired behaviour of a link and an EBF structure.

*Out-of-plane displacement*

The aim of this appraisal was to evaluate the potential localisation of intermediate stiffness in the web link and to prevent local buckling. Out-of-plane displacements were observed and their maximum values were placed as follows: for EBFs with links type HEA240, 260, 280, 300, 320, 340, 280, 300, and $t_{wL}/t_{wB} = 0.8$, the maximum deformation was placed near the left end of the web link.

Only EBFs with HEA360 and HEA400, and $t_{wL}/t_{wB} = 0.8$ presented the maximum deformation at mid-span, which coincides with the buckling mode. All EBFs with $t_{wL}/t_{wB} = 0.9$ exhibited the maximum values near the left end of the web link.

When $t_{wL}$ equals $t_{wB}$, EBFs with links type HEA240, 340, 360 and HEA400 located their maximum deformation near the left end of the web link and with HEA260, 280, 300 and HEA320, this value was placed near the right end of the web link (see Table 7).

Fig. 12 shows the displacement out of plane (U2 and U3) of the EBF with HEA360 link and $t_{wL} \ll t_{wB}$ (link web thickness of 8 mm, and beam and braces web thickness of 10 mm). The maximum deformation was placed in the middle of the web link. The curve in Fig. 12a presents a sudden change when the displacement applied was 68 mm, which represents the initiation of the shear failure.

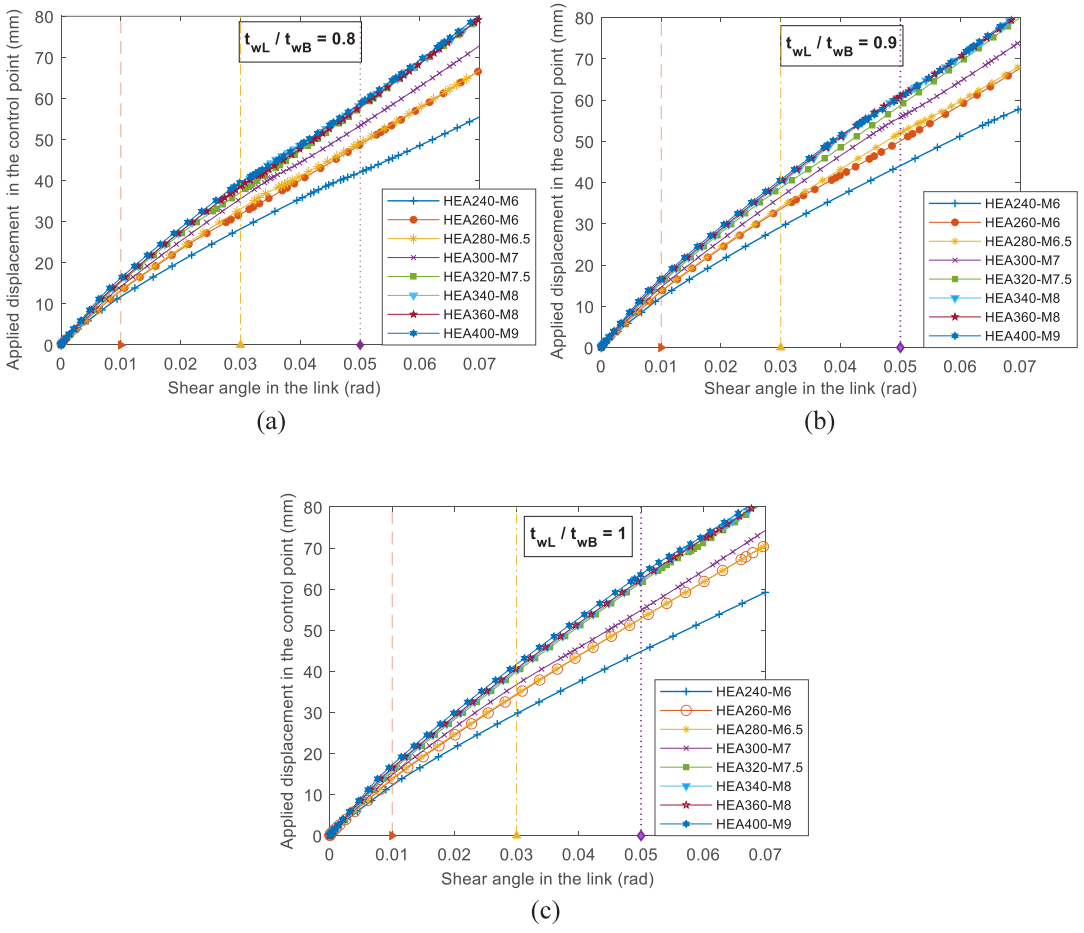


**Fig. 11.** Shear angle in the links due to the applied displacement.

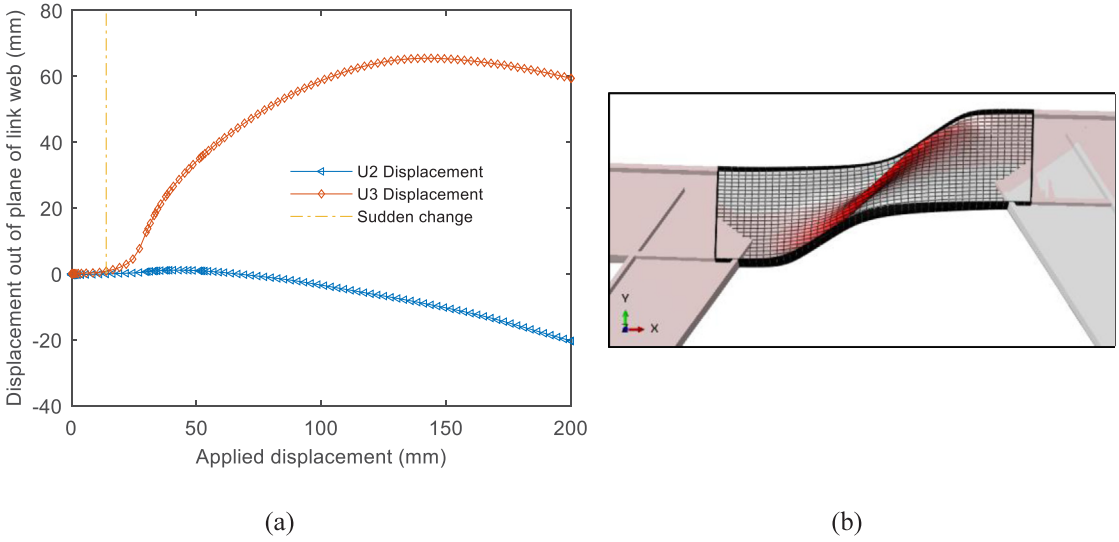


**Fig. 12.** Displacement out of plane of the link.

### 7.2. Inelastic dynamic analysis

This analysis was accomplished mainly to understand how the utilisation of cyclic parameters of austenitic SS influences the behaviour of the link and EBFs and the link overstrength.

*Yielding limit state*

The link elastic shear was analytically calculated and utilised as the benchmark, which was compared with the cyclic shear obtained from the numerical analysis in Abaqus and by the three variations of the use of cyclic parameters. According to the basic structure mechanics

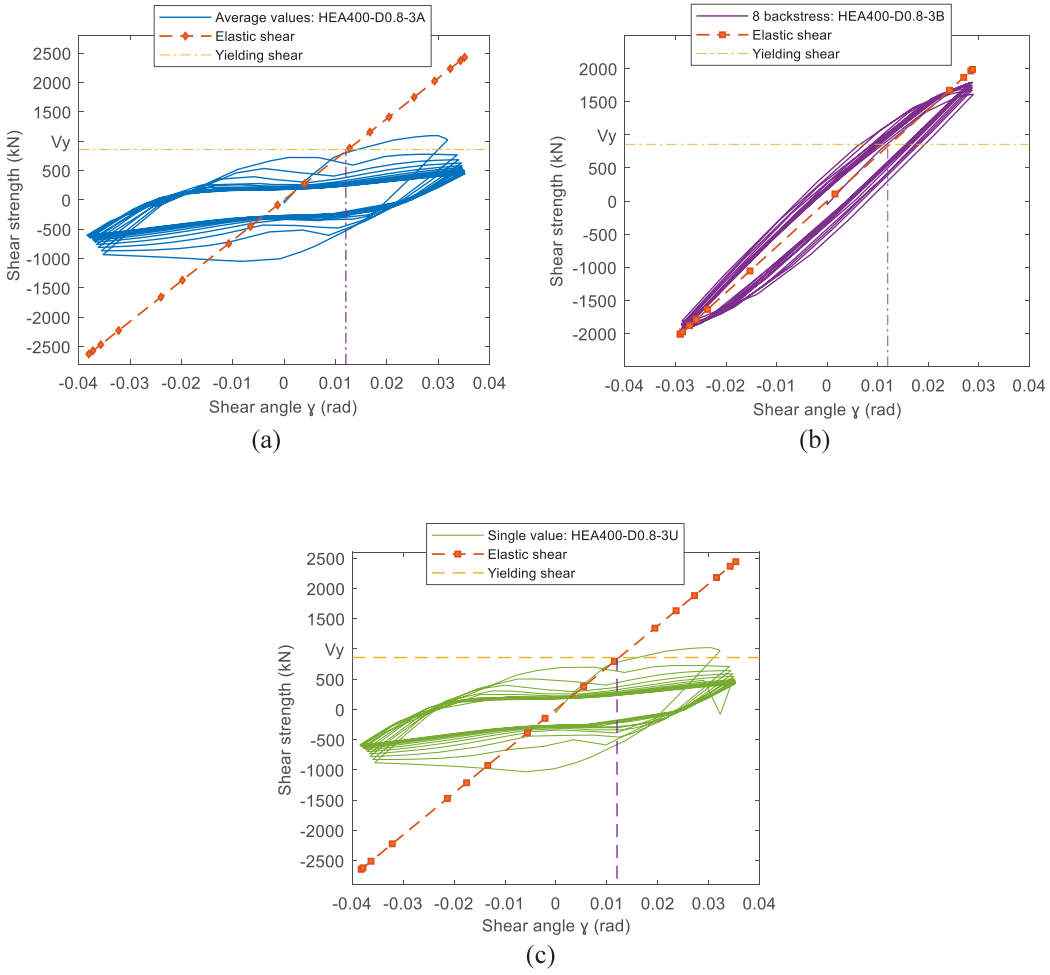


**Fig. 13.** Shear strength of the end link.

**Table 7**
Location of out of plane displacement.

| $t_{wL}/t_{wB}$ | Left | Middle | Right |
|---|---|---|---|
| 0.8 | HEA(240, 260, 320, 340, 280, 300) | HEA(360, 400) | - |
| 0.9 | HEA(240, 260, 280, 300, 320, 340, 360, 400) | - | - |
| 1 | HEA(240, 340, 360, 400) | - | HEA(260, 280, 300, 320) |

principle, the analytic stiffness stemmed from Eq. (2).

$$k_e = \frac{1}{\frac{1}{GA_V} + \frac{e^2}{12EI}} \tag{2}$$

where $e$ is the link length, $A_v$ is the shear area defined by $A_{v,EC3} = \left(A - 2b_f t_f + \left(t_w + 2r\right) t_f\right)$, $E$ is the Young's modulus, $I$ is the cross-sectional moment of inertia, and G is the shear modulus. Thus, the yielding displacement angle $\gamma_y$ of shear link is calculated by Eq. (3)

$$\gamma_y = \frac{V_y}{k_e} \tag{3}$$

$$V_y = 0.6 f_y A_{V,EC3} \tag{4}$$

The shear yielding strength can be determined by Eq. (4), where $f_y = 416.36$ MPA is the yielding strength defined in this study as the 0.2% of proof stress $\sigma_{0.2}$ of monotonic test in austenitic SS and the shear area equals $A_{v,EC3}$. The correct assumption of yielding shear limit proved to affect the link overstrength [13], and the $A_v$ was taken as $A_v = \left(d - t_f\right) t_w$ according to [13].

Table 8 summarises the results for the shear yielding strength of EBFs with all types of links.

Eq. (5) was applied to obtain the elastic shear strength $V_e$ (straight line in Fig. 13) of the links, where $\gamma_e$ is the shear angle in the elastic range. Given how small the shear angle is, it is determined by the ratio between the vertical displacement variation and the length link.

$$V_e = \gamma_e k_e \tag{5}$$

Results are available for 1%, 3% and 5%. Fig. 13 displays results for the applied constant strain amplitude applied 3%, which provides an interesting response. Based on the comparison of the three different forms in which the cyclic parameters are introduced into the model, the cyclic and elastic shears of EBFs with HEA400 and $t_{wL}/t_{wB} = 0.8$ are studied.

The following observations can be made (all EBFs of this example have the same geometrical and mechanical features):

- The assessment of the link with average values of cyclic parameters achieved one cycle and subsequently the strength dropped. The analytical elastic shear and the numerical response of the link were similar in the elastic range. However, the maximum analytical elastic shear was higher than the cyclic shear (Fig. 13a). The strain hardening is only noted in the first cycle.
- The link and the EBF with the superposition of eight backstresses reached the fifteen cycles applied without decreasing the shear strength. The strain hardening was clearly observed. The analytical elastic shear and the numerical response of the link were

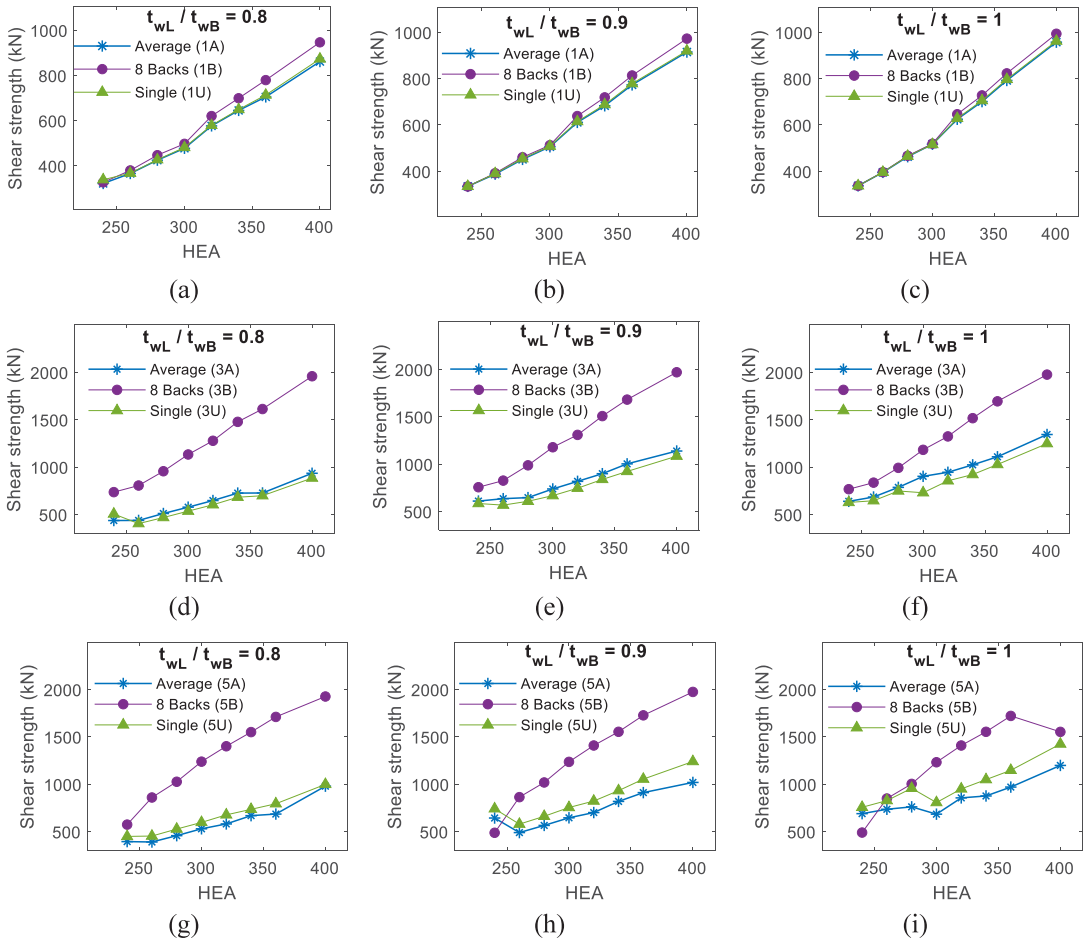


**Fig. 14.** Maximum shear strength achieved after cyclic protocol.

**Table 8**
Shear yielding strength of EBFs.

| Type | tw(mm) | Av (mm2) | Vy (kN) | $\gamma_y$ |
|---|---|---|---|---|
| HEA240 | 6 | 1368.00 | 341.75 | 0.009 |
| | 7 | 1596.00 | 398.71 | 0.010 |
| | 7.5 | 1710.00 | 427.19 | 0.011 |
| HEA260 | 6 | 1485.00 | 370.98 | 0.010 |
| | 7 | 1732.50 | 432.81 | 0.011 |
| | 7.5 | 1856.25 | 463.72 | 0.012 |
| HEA280 | 6.5 | 1735.50 | 433.56 | 0.009 |
| | 7.5 | 2002.50 | 500.26 | 0.010 |
| | 8 | 2136.00 | 533.61 | 0.011 |
| HEA300 | 7 | 2002.00 | 500.13 | 0.010 |
| | 8 | 2288.00 | 571.58 | 0.010 |
| | 8.5 | 2431.00 | 607.30 | 0.011 |
| HEA320 | 7.5 | 2283.75 | 570.52 | 0.011 |
| | 8.5 | 2588.25 | 646.59 | 0.012 |
| | 9 | 2740.50 | 684.62 | 0.012 |
| HEA340 | 8 | 2588.00 | 646.52 | 0.011 |
| | 9 | 2911.50 | 727.34 | 0.012 |
| | 9.5 | 3073.25 | 767.75 | 0.013 |
| HEA360 | 8 | 2740.00 | 684.50 | 0.011 |
| | 9.5 | 3253.75 | 812.84 | 0.013 |
| | 10 | 3425.00 | 855.62 | 0.013 |
| HEA400 | 9 | 3429.00 | 856.62 | 0.012 |
| | 10 | 3810.00 | 951.80 | 0.013 |
| | 11 | 4191.00 | 1046.98 | 0.014 |

similar in the elastic range and the maximum strength was barely higher than the cyclic response (Fig. 13b).

- The link analysis with the use of a single value for cyclic parameters, in this case for 3% of strain amplitude from experimental data, developed only one cycle and subsequently behaved similarly to the case of using average values as cyclic parameters (Fig. 13c).

*Shear strength in links*

Subsequently, the evaluation of the maximum shear force at the end of the links is evaluated.

- Fig. 14 (a,b and c) shows the maximum shear strength achieved after 12 cycles with 1% of applied strain. The form of utilisation of cyclic parameters had barely any influence in the shear strength. The links remained within the elastic range and no cyclic hardening was developed.
- When the applied strain amplitude was 3%, the influence of the cyclic parameters was higher (Fig. 14d, e and f); the maximum shear strength achieved almost the same results for the use of average and single values, while they were higher for the use of the superposition of eight backstresses. In this case, the maximum shear strength was obtained after the development of 12 cycles.
- When the applied strain amplitude was 5%, the cyclic hardening parameters influenced the maximum shear strength of links (Fig. 14 g, h and i). The lower results were performed for the use of average values, and the higher results were obtained for the use of superposition of eight backstresses. The cycles achieved were between three and five.

In both cases, for 3% and 5% of applied strain amplitude, the variation of the web thickness influenced accordingly the maximum

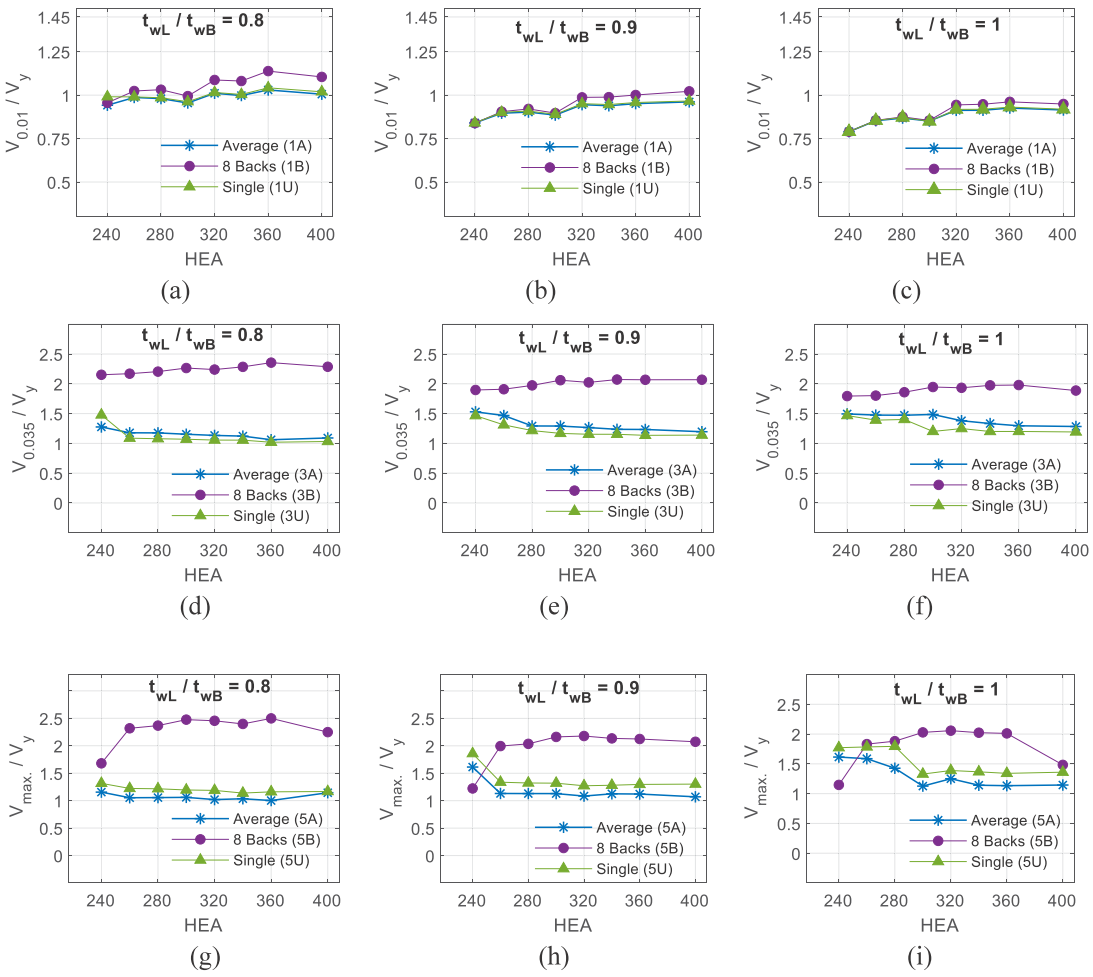


**Fig. 15.** Maximum-yielding shear strength ratio.

shear strength of links. Its influence on the stability of EBFs will be discussed later.

Therefore, the strong influence of the way of cyclic parameters are used was observed for models in the plastic stage and with stabilised cycles. The most conservative results regarding the link overstrength, were obtained through the superposition of eight backstresses, that resulted in greater hardening and greater forces.

*Ultimate-to-yielding strength ratio (plastic overstrength)*

According to the study performed by Xiaodong Ji et al. [15], the inelastic rotation of very short links was larger than shear links owing to the cyclic hardening effects of the web link, and the large shear strains developed were suspected to be a major cause of the increase of overstrength factor.

In this study, the ratio of the ultimate shear strength and the shear yielding strength was considered as the overstrength. The target was to observe the difference of results for the different variations of the designer-assumed cyclic parameters used, i.e. average values, superposition of eight backstresses and using a single measure value based on experimental data. Fig. 15 shows results on the ratio of the maximum shear strength and the yielding shear strength ($V_{0.01}/V_y$) for different link configurations. Where $V_{0.01}$ means the maximum shear strength reached, in this case, when the shear angle was 0.01 rad.

The maximum shear strength was achieved in $\gamma_{mean} = 0.01$ rad for 1%, $\gamma_{mean} = 0.035$ rad for 3% and $\gamma_{mean} = 0.053$ rad for 5% of applied strain amplitude, where $\gamma_{mean}$ is the average maximum shear angle for each applied strain amplitude. All models with 1% and 3% of applied strain amplitude showed a maximum shear angle near the $\gamma_{mean}$. However, when the strain amplitude was 5%, the shear angle was approximately 0.042rad when the superposition of eight backstresses was used and 0.060 rad when the average and single values were used.

Repeatedly, the results showed that when the applied strain amplitude was 1%, the links worked in their elastic states without passing the yielding shear strength. For small values of $t_{wL}/t_{wB} = 0.8$, the peak shear exceeded the yielding shear strength and the maximum overstrength was 1.15 (Fig. 15a, b and c).

When the strain amplitude was 3% the difference in the use of cyclic parameters was evident (Fig. 15d, e and f). The overstrength, which increased by 100% of the yielding shear, were higher when the superposition of eight backstresses were applied, in contrast, for the average and single cyclic parameters, the obtained ratios were lower.

When the applied strain amplitude was 5% (Fig. 15 g, h and i)., the smallest ratios were obtained for the case of average values of cyclic parameters with an increase in 20% in all the EBFs. 30% increase was noted for the single values of cyclic parameters and, the highest ratios were again observed when eight backstresses were assumed (values greater than 100% increase).

On the other hand, the maximum shear angle ($\gamma_{max}$) also suffered a slight variation by the way cyclic parameters are used. The higher displacements were found for the cases of average and single values of cyclic parameters, while the results obtained by the superposition of eight backstresses were smaller.

Fig. 16 illustrates the variation of the maximum shear angle in each model, which demonstrates the aforementioned paragraph.

*Horizontal reaction of EBFs*

The horizontal reaction in the control point was extracted from all models. The following results are worth pointing out.

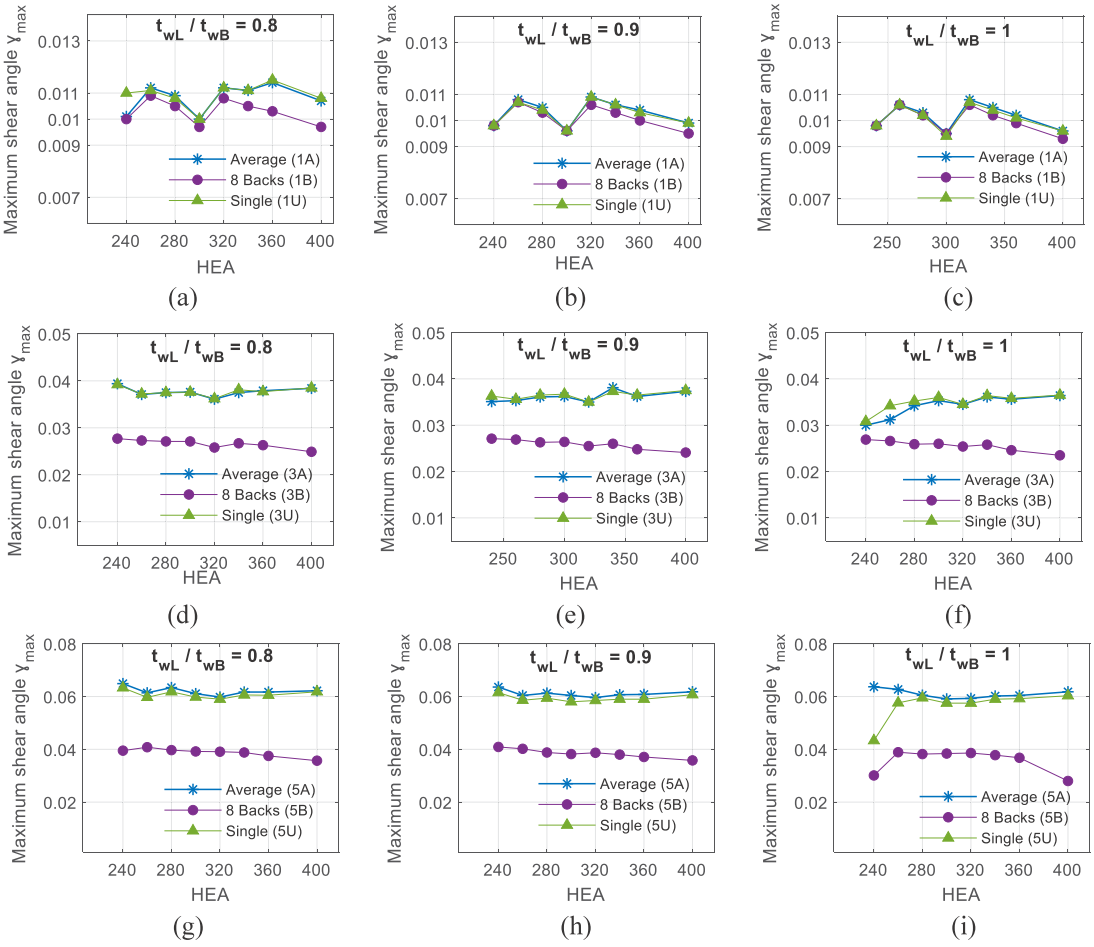


**Fig. 16.** Maximum shear angle in each model.

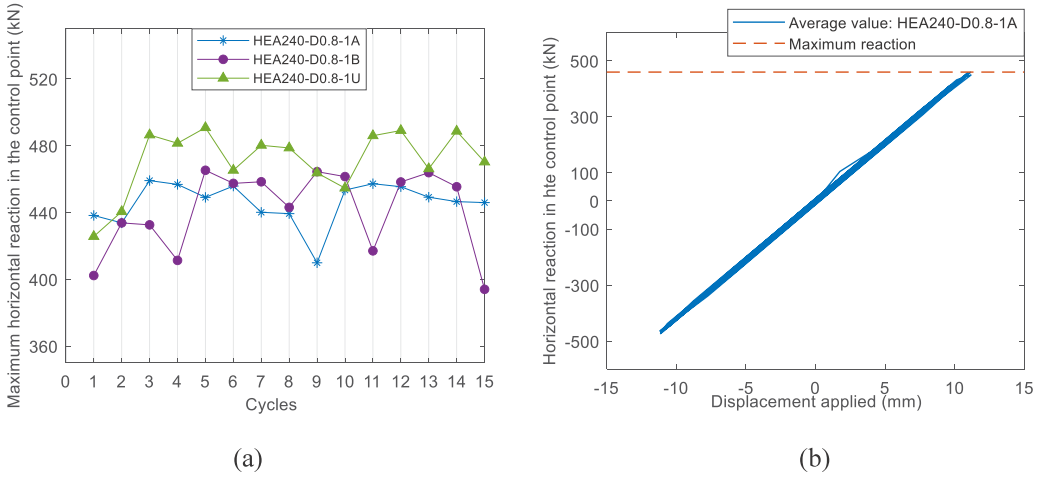


**Fig. 17.** Comparison of hysteresis curves of HEA240-D0.8–1 A, HEA240-D0.8-1B and HEA240-D0.8-1U.

When the strain amplitude was 1%, EBFs with $t_{wL} \ll t_{wB}$ developed the elastic range, with barely dissipated energy (Fig. 17a and b). EBFs with $t_{wL} < t_{wB}$ and $t_{wL} = t_{wB}$ remained in the elastic range, which was an evident response because the thickness of the link was higher.

When the applied strain amplitude was 3%, all EBFs achieved the plastic stage; however, a great difference between hysteresis curves due to the form of utilisation of cyclic hardening parameters was observed.

Fig. 18 (a, b and c) exhibits displacement-reaction curves for three models with equal geometrical and material configurations with the unique difference of the cyclic hardening parameters. Fig. 18a shows the EBF with the average values (average from 0.75% to 5% of strain amplitude) of cyclic parameters (Table 5b). Fig. 18b shows the same model with the superposition of eight backstresses in kinematic hardening by referring to Table 6b. Fig. 18c draws the same EBF with single values of cyclic parameters, in this case values for 3% of strain amplitude (Table 6a).

Hysteresis curves are almost similar for the assumption of single values and average values of cyclic parameters. In contrast, the adoption of

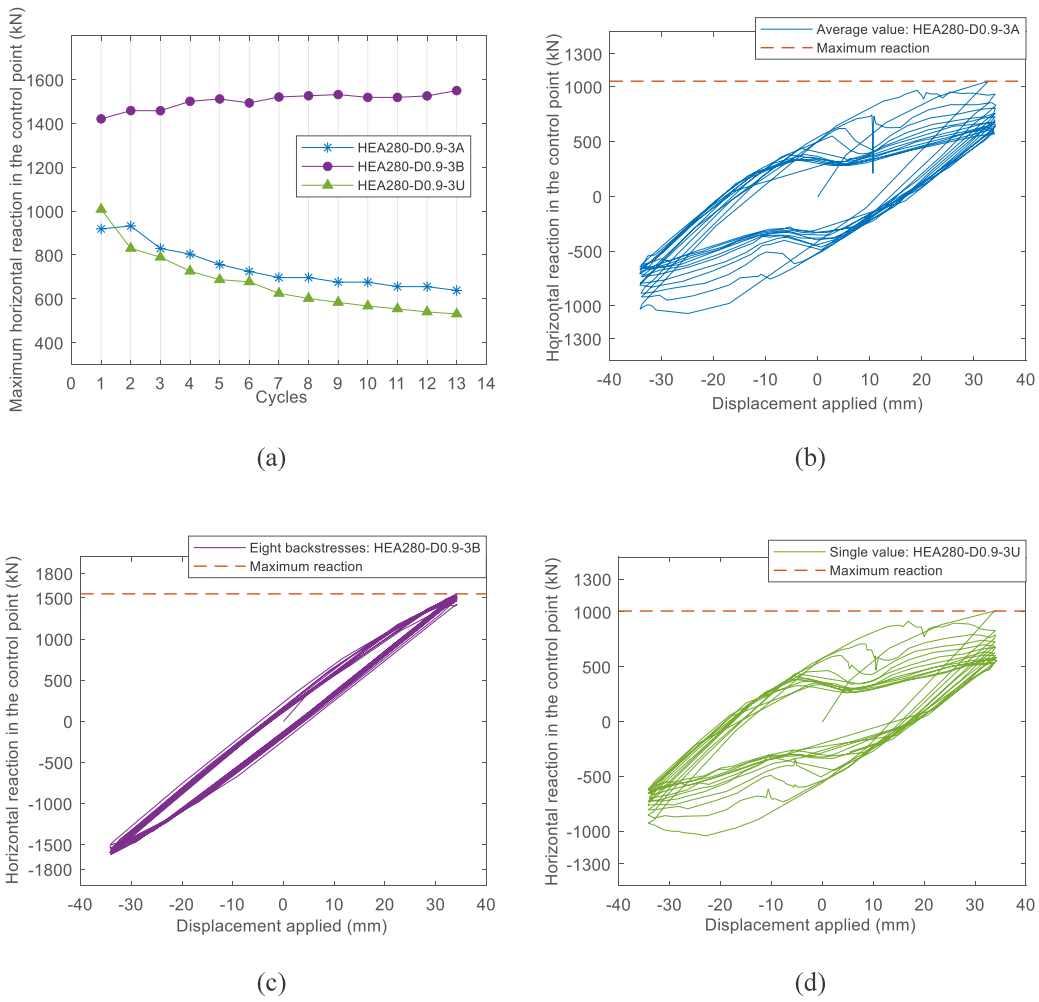


**Fig. 18.** Comparison of hysteresis curves of HEA280-D0.9–3 A, HEA240-D0.9-3B and HEA240-D0.9-3U.

the superposition of eight backstresses displays a significant variation in dissipated energy, and maximum reaction force.

Additionally, a comparison between the maximum horizontal reactions achieved in each cycle was evaluated (Fig. 18a). The strain hardening is observed in the first cycles for single values, it reaches eight cycles for the use of average values and it is steadily increasing when the superposition of eight backstresses is applied.

When the strain amplitude was 5%, all EBFs presented shear failure mechanism after approximately five cycles. For average and single values, the EBFs failed after approximately three cycles; nevertheless, when eight backstresses were superposed, EBFs failed after approximately four cycles. Fig. 19 (a, b and c) shows the displacement-reaction forces.

In Fig. 19a, the cyclic hardening is observed; again, the higher results were reached when the superposition of eight backstresses was employed.

The way of cyclic parameters are assumed also influences the global stability of the EBF. Fig. 20 draws the final stage of the EBF after four cycles with 5% of applied strain amplitude and the shear angles larger than 0.08 rad. The geometry and material properties are similar in all cases. Fig. 19a and c show the local buckling developed by the links when average and single values of cyclic parameters were used. Localised damage on the link (whose overstrength was lower) did not affect the surroundings. However, when the superposition of eight backstresses was utilised and the forces were higher, the surroundings were also affected and global instability was observed in the EBF (Fig. 20b).

It is of an utmost importance in design, to select an adequate factor for the overstrength. From Eq. (1), two factors are included in design for accounting for the increase of response during seismic episodes: one is related to the nominal yield stress (intrinsic material overstrength) and the other, to the strain hardening effect of the material.

A suitable set of cyclic hardening parameters and proposed values for both overstrength factors in EBFs with austenitic SS links are required in design. Presently, other studies including statistics and including vaster systems (EBFs) are being carried out by the authors in order to present a more comprehensive proposal for such design values.

In order to recommend specific cyclic parameters to select, it is necessary to evaluate the load applied, the ductility, and the overstrength final. At the material level, when the kinematic hardening was regular, the numerical results showed a high ductility and good agreement with the experimental data. The element and simple structure level, when the kinematic hardening was regular the structure achieved a few cycles before the failure and when 8 backstresses were used the structure achieved higher strength with the consequent increase of the overstrength.

### 7.3. Evaluation of a eccentrically braced frame

Finally, a case of EBF with five storeys and one span was developed to confirm the previous results. This structure was studied from the geometrical configuration of the reference [40].

The sections adopted were those that ensured the serviceability limit state. Furthermore, it was used IPE type of cross section in

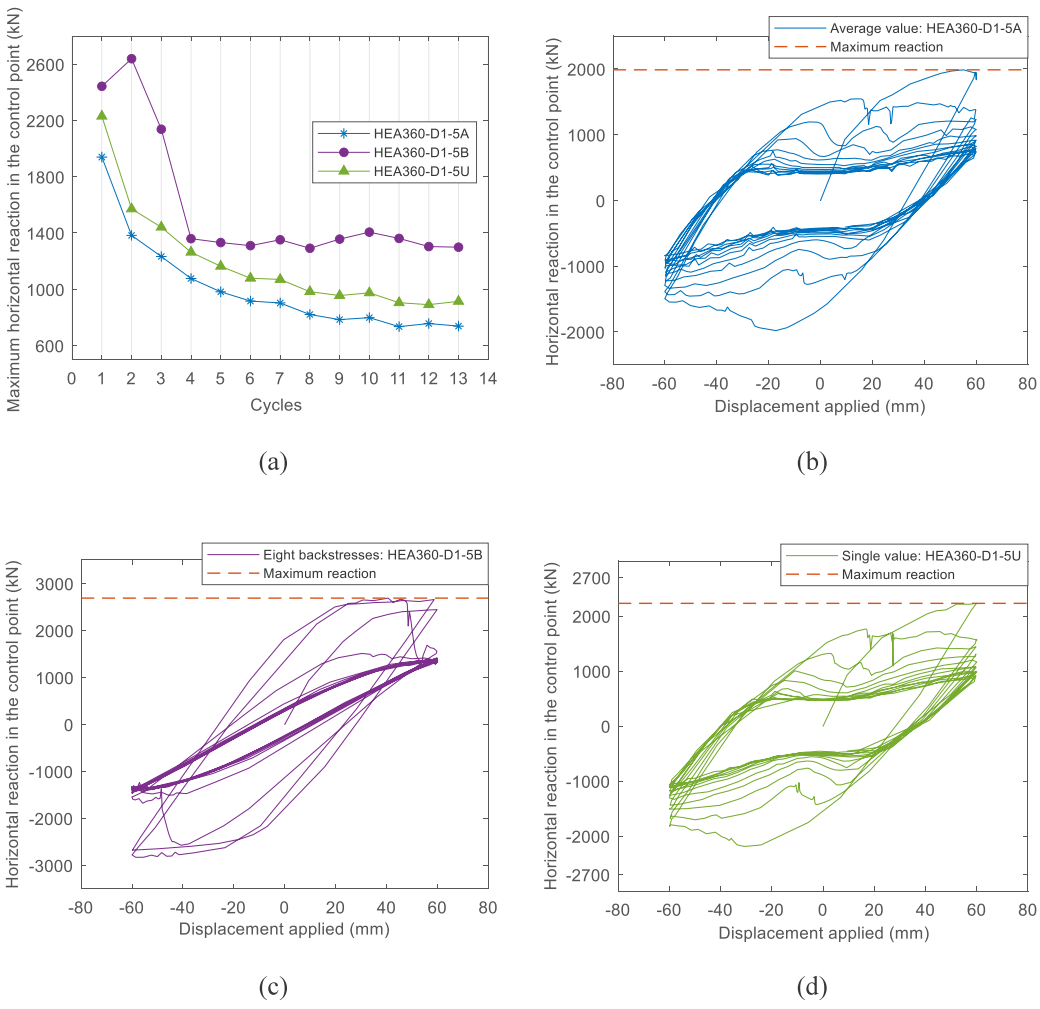


**Fig. 19.** Comparison of hysteresis curves of HEA360-D1.0–5 A, HEA360-D1.0-5B and HEA360-D1.0-5U.

beams and links and in braces of the last storey. Beams, braces and columns were of carbon steel and links were of austenitic stainless steel studied in previous items in such way that the influence of the designer-assumption of the cyclic parameters can be observed.

Fig. 21 shows the geometry, sections used and. Further, permanent and quasi-permanent loads were applied in a first step, the inertial mass was applied in corners of the EBF as well. In a second step, horizontal incremental loads in each storey was applied (Fig. 21), which represent the form of the fundamental mode of vibration.

From the second step, a pushover curve was obtain.

From the pushover curve (Fig. 22) equivalent displacements to $\Delta_p/h = 0.2\%$ and 1% was selected, where $\Delta_p$ is the storey drift produced by the horizontal displacement applied, and h is the total height of the building.

The third step consisted in the application of a cyclic horizontal displacement with amplitudes corresponding to 0.2% and 1% from the previous step. For each displacement selected, three different ways to apply the cyclic parameters of the austenitic stainless steel was applied.

Displacement equivalent to 0.2%

When the cyclic displacement applied was 0.2% of amplitude, the structure behaved near the elastic range. The hysteresis curves showed a few dissipation of energy, and the maximum horizontal reaction in the base was almost similar in each way of designer-assumption of the cyclic parameters selected (Fig. 23).

It is worth to point that the displacement applied corresponding to a zone close to elastic range, and therefore, the influence of the cyclic behaviour of whole structure is not noticeable.

Displacement equivalent to 1%

For this displacement, the influence of the designer-assumption is relevant. When eight kinematic strain hardening was applied, the hysteresis curve showed a better form and the strain hardening can be clearly observed. However, the force achieved was higher with almost 1.5 times than the other two ways Fig. 24.

When the average values and a value corresponding to 1% of strain amplitude of the cyclic parameters were applied, the structure achieve only one cycle and in the second cycle a shear failure of the first link was observed.

These results confirm the previous analysis. Therefore, it is necessary to consider a detail the selection of the cyclic parameters at material level, mainly by the higher influence in design parameters as the overstrength of elements that dissipate energy.

## Conclusions

The main target of this study was the analysis of the influence of the cyclic parameters on the overstrength of shear link and the cyclic behaviour of EBFs. This study conducted a parametric study of 216 numerical models of hybrid EBFs subjected to constant cyclic strain. Through the obtained results, one key aspect for practical design is pointed out. The overstrength of austenitic SS links depends considerably on the designer-assumed selected values for numerical modelling of the cyclic response. In Higher forces and higher dissipation of energy was found when several (eight) backstresses were selected for the kinematic hardening modelling. When analysing overstrength and how this

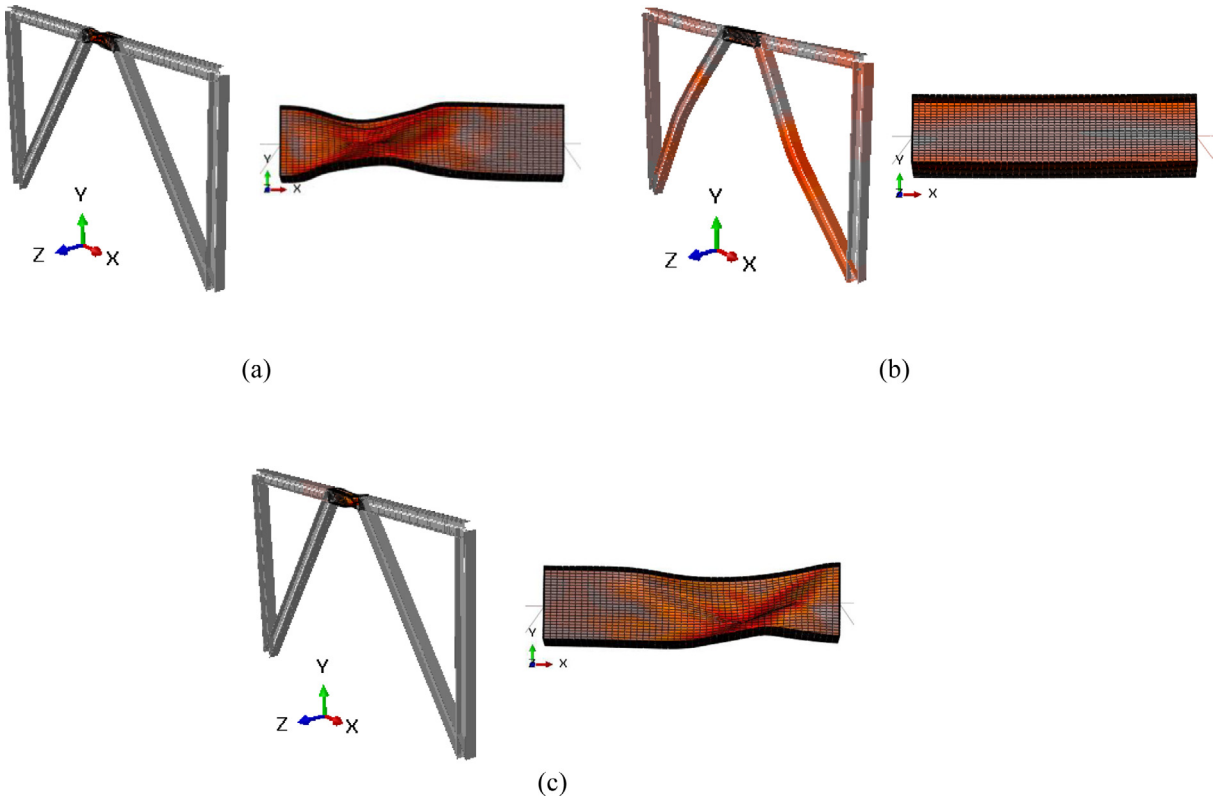


**Fig. 20.** Global and local buckling after four cycles of 5% of strain amplitude.

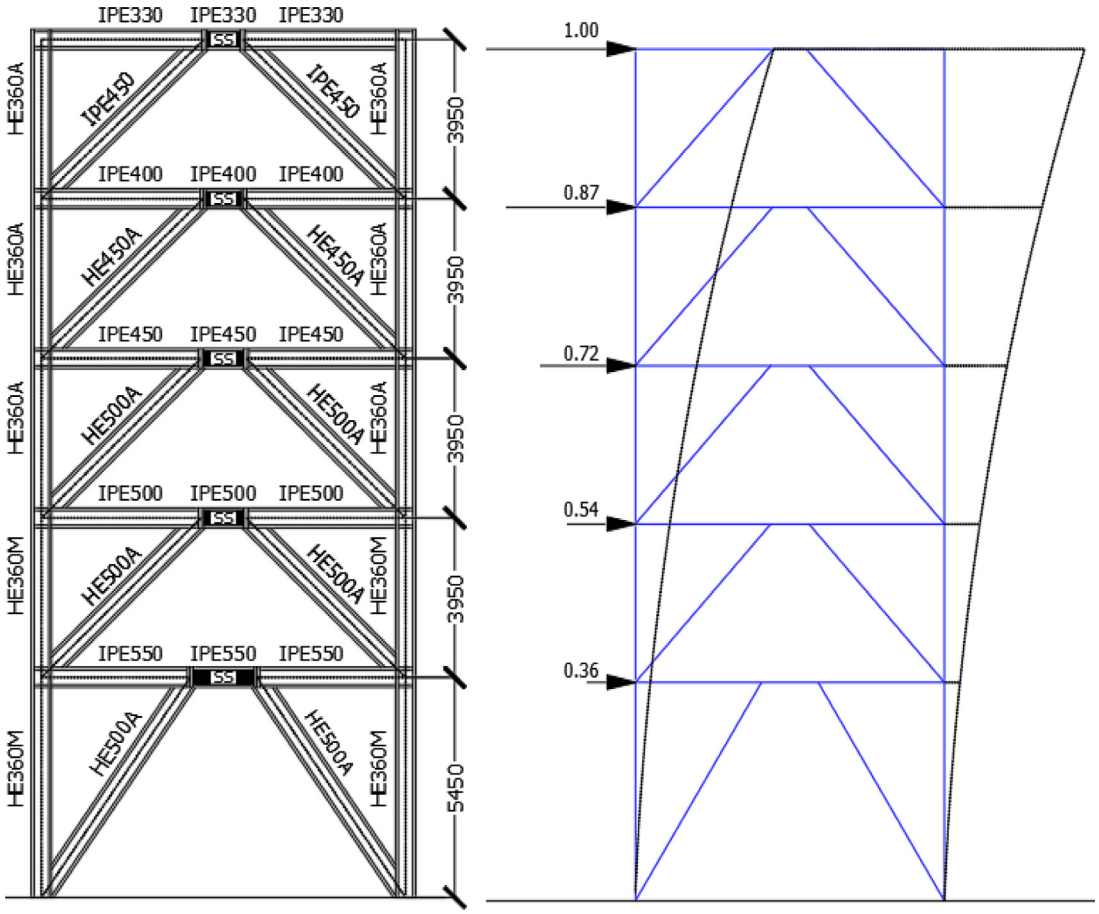


**Fig. 21.** Geometry of the EBF (measures are in mm) and fundamental mode of vibration.

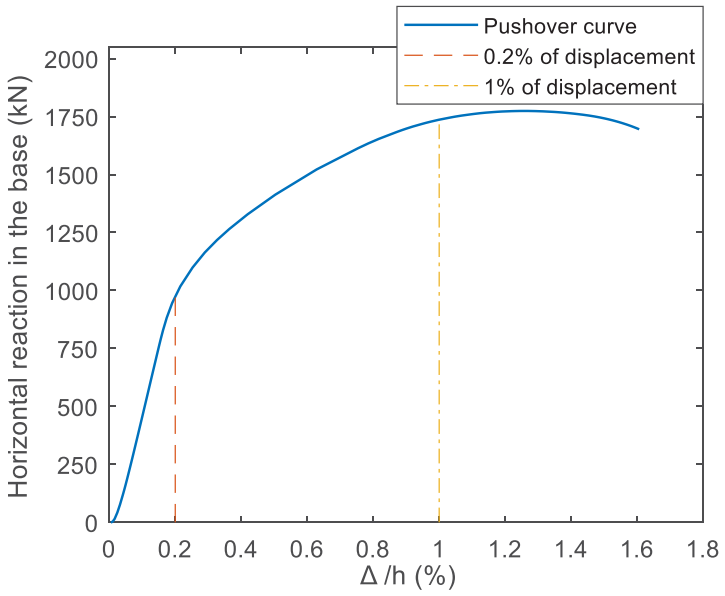


**Fig. 22.** Pushover curve due to the fundamental mode of vibration.

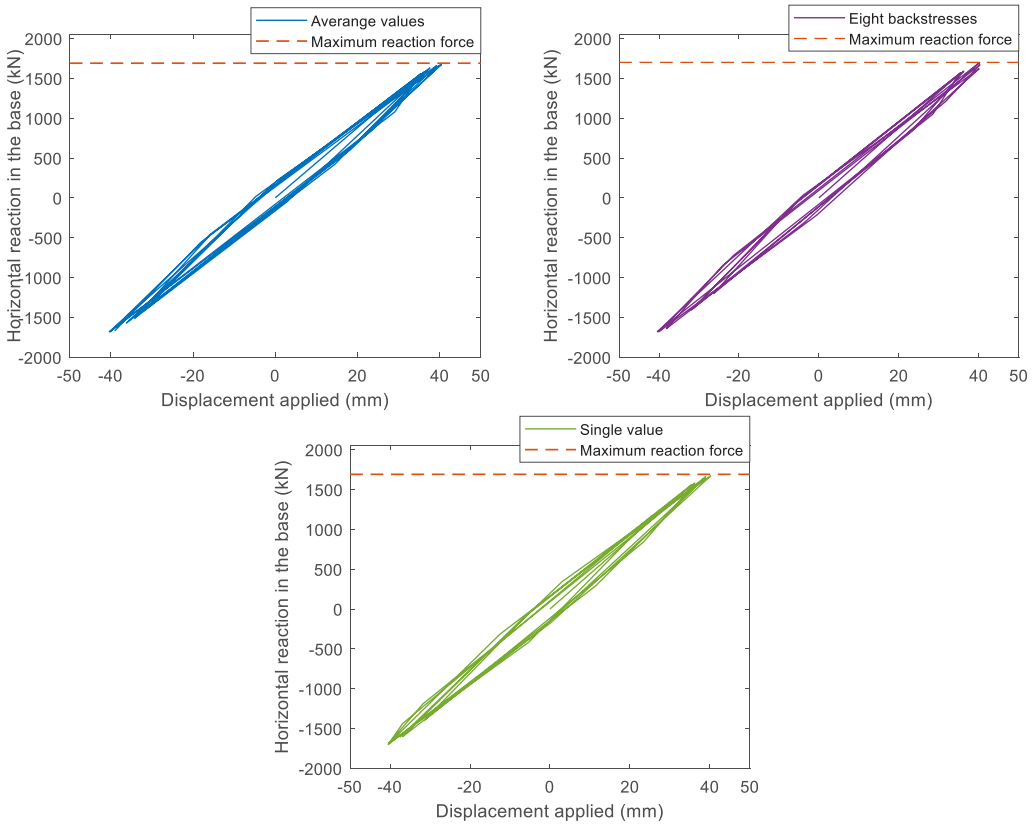


**Fig. 23.** Comparison of hysteresis curves of 0.2% of strain amplitude applied.

affects the surrounding of the dissipative zones, the use of backstresses results on more conservative results for design purposes. It is also seen that the selection of such values may depend on the knowledge of the response the designer may have. As a result, design becomes iterative. A thorough analysis of the design values for overstrength (nominal yield stress and strain hardening) are necessary for EBFs assembled with SS links. Further studies including different geometrical configurations for EBFs as well as targeting the effect of the migration of the forces of the links to their surroundings (to non-dissipative zones) are under development.

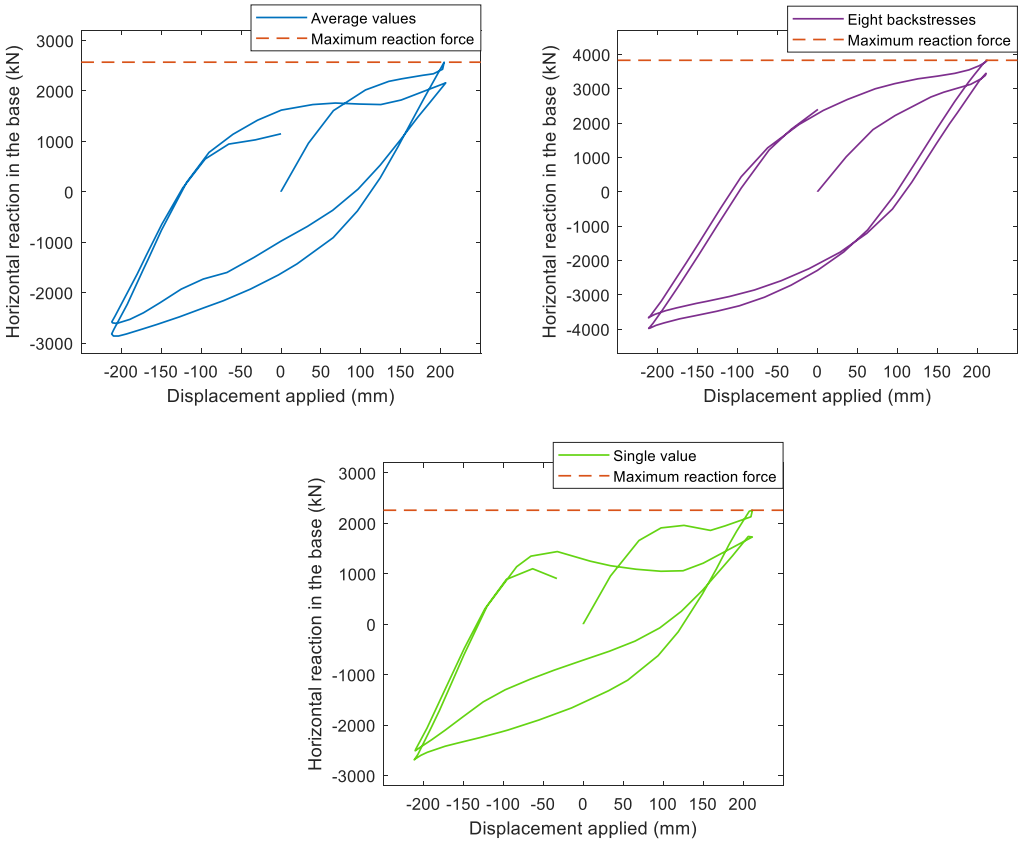


**Fig. 24.** Comparison of hysteresis curves of 1% of strain amplitude applied.

## CRediT authorship contribution statement

**Lucy Lázaro:** Conceptualization, Methodology, Data curation, Writing – original draft. **Rolando Chacón:** Methodology, Supervision, Writing – review & editing.

## Declaration of competing interest

The authors declare that they have no known competing financial interests or personal relationships that could have appeared to influence the work reported in this paper.

## Data availability

Data will be made available on request.

## Acknowledgements

The authors acknowledge the financial support provided by the Project BIA2016-75678-R, AEI/FEDER, UE "*Comportamiento estructural de pórticos de acero inoxidable. Seguridad frente a acciones accidentales de sismo y fuego*", funded by the Spanish Ministry of Economic Affairs and Digital Transformation (MINECO). The first author acknowledges the financial support from the Peruvian Government *Beca Generación del Bicentenario*.

## References

[1] K.H. Nip, L. Gardner, C.M. Davies, A.Y. Elghazouli, Extremely low cycle fatigue tests on structural carbon steel and stainless steel, J. Construct. Steel Res. 66 (2010) 96–110, http://dx.doi.org/10.1016/j.jcsr.2009.08.004.

[2] S. Chandra, S. Goyal, R. Sandhya, S.K. Ray, Low cycle fatigue life prediction of 316 L ( N ) stainless steel based on cyclic elasto-plastic response, Nucl. Eng. Des. 253 (2012) 219–225, http://dx.doi.org/10.1016/j.nucengdes.2012.08.024.

[3] V. Mazánová, V. Škorík, T. Kruml, J. Polák, Cyclic response and early damage evolution in multiaxial cyclic loading of 316L austenitic steel, Int. J. Fatigue 100 (2017) 466–476, http://dx.doi.org/10.1016/j.ijfatigue.2016.11.018.

[4] I. González-de león, E. Nastri, I. Arrayago, R. Montuori, Experimental study on stainless steel tubular members under cyclic loading, Thin-Walled Struct. 181 (2022) http://dx.doi.org/10.1016/j.tws.2022.109969.

[5] J.D. Gao, X.X. Du, H.X. Yuan, M. Theofanous, Hysteretic performance of stainless steel double extended end-plate beam-to-column joints subject to cyclic loading, Thin-Walled Struct. 164 (2021) http://dx.doi.org/10.1016/j.tws.2021.107787.

[6] I. Arrayago, I. González-de León, E. Real, E. Mirambell, Tests on stainless steel frames. Part I: Preliminary tests and experimental set-up, Thin-Walled Struct. 157 (2020) http://dx.doi.org/10.1016/j.tws.2020.107005, (art. no. 107005).

[7] I. Arrayago, I. González-de León, E. Real, E. Mirambell, Tests on stainless steel frames. Part II: Results and analysis, Thin-Walled Struct. 157 (2020) http://dx.doi.org/10.1016/j.tws.2020.107006, (art. no. 107006).

[8] Y. Shen, R. Chacón, Flexural stiffness reduction for stainless steel SHS and RHS members prone to local buckling, Thin-Walled Struct. 155 (2020) http://dx.doi.org/10.1016/j.tws.2020.106939, (art. no. 106939).

[9] Y. Shen, R. Chacón, Geometrically non-linear analysis with stiffness reduction for the stability design of stainless steel structures: Application to members and planar frames, Thin-Walled Struct. 148 (2020) http://dx.doi.org/10.1016/j.tws.2019.106581.

[10] Eurocode 8: Design of Structures for Earthquake Resistance Part1:General Rules, Seismic Actions and Rules for Buildings, European Comitee for Standardisation, 2004.

[11] AISC, Seismic Provisions for Structural Steel Buildings, Standard ANSI/AISC 341-16, American Institute of Steel Construction, Chicago (IL), Chicago (IL), 2016.

[12] X. Liu, J. Fan, Y. Liu, M. Zheng, J. Nie, Theoretical research into cyclic web buckling and plastic overstrength of shear links, Thin-Walled Struct. 152 (2020) http://dx.doi.org/10.1016/j.tws.2020.106644, (art. no. 106644).

[13] G. Della Corte, M.D. Aniello, R. Landolfo, Analytical and numerical study of plastic overstrength of shear links, J. Construct. Steel Res. 82 (2013) 19–32, http://dx.doi.org/10.1016/j.jcsr.2012.11.013.

[14] Kazemzadeh Azad, C. Topkaya, A review of research on steel eccentrically braced frames, J. Construct. Steel Res. 128 (2017) 53–73, http://dx.doi.org/10.1016/j.jcsr.2016.07.032.

[15] X. Ji, Y. Wang, Q. Ma, T. Okazaki, Cyclic behavior of very short steel shear links, J. Struct. Eng. 142 (2016) http://dx.doi.org/10.1061/(ASCE)ST.1943-541X.0001375, (art. no. 04015114).

[16] Y.O. Ozk, Interaction of flange and web slenderness, overstrength factor and proposed stiffener arrangements for long links, J. Construct. Steel Res. 190 (2022) http://dx.doi.org/10.1016/j.jcsr.2022.107150, (art. no. 107150).
[17] T. Okazaki, M.D. Engelhardt, Cyclic loading behavior of EBF links constructed of ASTM A992 steel, J. Construct. Steel Res. 63 (2007) 751–765, http://dx.doi.org/10.1016/j.jcsr.2006.08.004.
[18] L. Manganiello, R. Montuori, E. Nastri, V. Piluso, The influence of the axial restraint on the overstrength of short links, J. Construct. Steel Res. 184 (2021) http://dx.doi.org/10.1016/j.jcsr.2021.106758, (art. no. 106758).
[19] A. Mohebkhah, B. Chegeni, Overstrength and rotation capacity for EBF links made of European IPE sections, Thin-Walled Struct. 74 (2014) 255–260, http://dx.doi.org/10.1016/j.tws.2013.10.013.
[20] W. Yin, F. Sun, H. Jin, D. Hu, Experimental and analytical study on plastic overstrength of shear links covering the full range of length ratio, Eng. Struct. 220 (2020) http://dx.doi.org/10.1016/j.engstruct.2020.110961, (art. no. 110961).
[21] J.L. Chaboche, A review of some plasticity and viscoplasticity constitutive theories, Int. J. Plast. 24 (2008) 1642–1693, http://dx.doi.org/10.1016/j.ijplas.2008.03.009.
[22] J.L. Chaboche, Constitutive equations for cyclic plasticity and cyclic viscoplasticity, Int. J. Plast. 5 (1989) 247–302.
[23] L. Lazaro, R. Chacón, Material behaviour of austenitic stainless steel subjected to cyclic and arbitrary loading, J. Constr. Steel Res. 189 (2022) http://dx.doi.org/10.1016/j.jcsr.2021.107113, (art. no. 107113).
[24] S. Zheng, F. Zhou, J. Cheng, H. Li, R. Rong, Experimental study on cyclic hardening characteristics of structural stainless steels, J. Construct. Steel Res. 191 (2022) http://dx.doi.org/10.1016/j.jcsr.2022.107196, (art. no. 107196).
[25] L. DiSarno, A.S. Elnashai, D.A. Nethercot, Seismic response of stainless steel braced frames, J. Construct. Steel Res. 64 (2008) 914–925, http://dx.doi.org/10.1016/j.jcsr.2008.01.027.
[26] R. Li, Y. Zhang, L.W. Tong, Numerical study of the cyclic load behavior of AISI 316L stainless steel shear links for seismic fuse device, Front. Struct. Civ. Eng. 8 (2014) 414–426, http://dx.doi.org/10.1007/s11709-014-0276-4.
[27] R. Chacón, A. Vega, E. Mirambell, Numerical study on stainless steel I-shaped links on eccentrically braced frames, J. Construct. Steel Res. 159 (2019) 67–80, http://dx.doi.org/10.1016/j.jcsr.2019.04.014.
[28] Y. Wu, S. Fan, Y. Guo, S. Duan, Q. Wu, Experimental study and numerical simulation on the seismic behavior of diagonally stiffened stainless steel plate shear walls under low cyclic loading, Thin-Walled Struct. 182 (2023) 110165, http://dx.doi.org/10.1016/j.tws.2022.110165.
[29] K.J.R. Rasmussen, Full-range stress–strain curves for stainless steel alloys, J. Construct. Steel Res. 59 (2003) 47–61.
[30] J.D. Gao, H.X. Yuan, H. Qian, X.W. Chen, Structural behaviour and design of stainless steel end-plate beam-to-exterior column minor-axis joints, Thin-Walled Struct. 181 (2022) 110119, http://dx.doi.org/10.1016/j.tws.2022.110119.
[31] X. Chang, L. Yang, M. Wang, F. Yin, Study on constitutive model of austenitic stainless steel and duplex stainless steel under cyclic loading, Eng. Mech. 36 (2019) 137–147, http://dx.doi.org/10.6052/j.issn.1000-4750.2018.03.0184.
[32] M. Bastami, R. Ahmady Jazany, A. Mohamadi, Study of the seismic performance of Centrically Fused Braced Frame (CFBF), Thin-Walled Struct. 145 (2019) 106401, http://dx.doi.org/10.1016/j.tws.2019.106401.
[33] M. Bastami, R. Ahmady Jazany, Development of centrically fused braced frame (CFBF) for seismic regions, Soil Dyn. Earthq. Eng. 127 (2019) 105856, http://dx.doi.org/10.1016/j.soildyn.2019.105856.
[34] M. Bastami, R. Ahmady Jazany, Development of Eccentrically Interconnected Braced Frame (EIC-BF) for seismic regions, Thin-Walled Struct. 131 (2018) 451–463, http://dx.doi.org/10.1016/j.tws.2018.07.021.
[35] Design Manual for Structural Stainless Steel, fourth ed., Steel Construction Institute, 2017.
[36] Eurocode 3: Design of Steel Structures - Part 1-1: General Rules and Rules for Buildings, European Comitee for Standardisation, 2005.
[37] A. Dutta, S. Dhar, S.K. Acharyya, Material characterization of SS 316 in low-cycle fatigue loading, J. Mater. Sci. 45 (2010) 1782–1789, http://dx.doi.org/10.1007/s10853-009-4155-7.
[38] R.A. Chacon, M.D. De Marco, E. Real, I. Arrayago, Experimental study on the cyclic response of austenitic stainless steel, in: 14th World Conf. Earthq. Eng, Vol. 9, 2018, http://dx.doi.org/10.18057/ICASS2018.P.080.
[39] S.H. Heng, M.S.M. Azmi, M.A. Rojan, M.S.M. Hashim, M.N. Ayob, A.H. Ismail, M.S.A. Manan, S. Abdullah, Effect of loading protocol on the mechanical properties of 316L stainless steel, J. Phys. Conf. Ser. 2051 (2021) http://dx.doi.org/10.1088/1742-6596/2051/1/012029, (art. no. 012029).
[40] M. Bruneau, C.-M. Uang, R. Sabelli, Ductile desing of steel structures, 2011.
[41] ABAQUS, ABAQUS/CAE User's Manual and ABAQUS CAE Manual, Simulia Dassault Systèmes, 2017.
[42] Eurocode 3: Design of Steel Structures - Part 1-5: Plated Structural Elements, European Comitee for Standardisation, 2006.
[43] P.W. Richards, C.-M. Uang, Effect of flange width-thickness ratio on eccentrically braced frames link cyclic rotation capacity, J. Struct. Eng. 131 (2005) 1546–1552, http://dx.doi.org/10.1061/(asce)0733-9445(2005)131:10(1546).